

Inferring redshift and energy distributions of fast radio bursts from the first CHIME/FRB catalog^{*}

Li Tang¹ Hai-Nan Lin^{2,3;1)} Xin Li^{2,3}

¹ Department of Math and Physics, Mianyang Teachers' College, Mianyang 621000, China

² Department of Physics, Chongqing University, Chongqing 401331, China

³ Chongqing Key Laboratory for Strongly Coupled Physics, Chongqing University, Chongqing 401331, China

Abstract: We reconstruct the extragalactic dispersion measure – redshift relation ($DM_E - z$ relation) from well-localized fast radio bursts (FRBs) using Bayesian inference method. Then the $DM_E - z$ relation is used to infer the redshift and energy of the first CHIME/FRB catalog. We find that the distributions of extragalactic dispersion measure and inferred redshift of the non-repeating CHIME/FRBs follow cut-off power law, but with a significant excess at the low-redshift range. We apply a set of criteria to exclude events which are susceptible to selection effect, but find that the excess at low redshift still exists in the remaining FRBs (which we call Gold sample). The cumulative distributions of fluence and energy for both the full sample and the Gold sample do not follow the simple power law, but they can be well fitted by the bent power law. The underlying physical implications remain to be further investigated.

Key words: fast radio bursts – intergalactic medium – cosmological parameters

1 Introduction

Fast radio bursts (FRBs) are energetic radio pulses of milliseconds duration happening in the Universe, see e.g. [1–4] for recent review. The discovery of the first FRB can date back to 2007, when Lorimer et al. [5] reanalyzed the 2001 archive data of the Parkes 64-m telescope and found an anomalous radio pulse, which is now named FRB010724. Later on, Thornton et al. [6] discovered several other similar radio pulses, which made FRBs receive great attention within the astronomy community. The origin of FRBs was still a mystery at that time, but the large dispersion measure (DM) implies that they are unlikely to originate from the Milky Way. The identification of host galaxy and the direct measurement of redshift confirmed that they have an extragalactic origin [7–9]. Up to now, several hundreds of FRBs have been discovered [10, 11], among which only one is confirmed to originate from our Galaxy [12]. Phenomenological, FRBs can be divided into two types: repeaters and non-repeaters, according to whether they are one-off events or not. The majority of FRBs are apparently non-repeating, but it is still unclear if they will be repeating in the future. Most repeating FRBs are not very active, which repeat only two to three times [13]. However, more than one thousand bursts have been observed from two extremely active sources, i.e. FRB20121102A

[14] and FRB20201124A [15].

The physical origin of FRBs is still under extensive debate. Several theoretical models have been proposed to explain repeating and non-repeating FRBs, respectively. For example, giant pulses from young rapidly rotating pulsars [16], the black hole battery model [17], the “Cosmic Comb” model [18], the inspiral and merger of binary neutron stars [19, 20], neutron star-white dwarf binary model [21], collision between neutron stars and asteroids [22], highly magnetized pulsars travelling through asteroid belts [23, 24], young magnetars with fracturing crusts [25], axion stars moving through pulsar magnetospheres [26], and so on. Although there is no standard model yet, it is widely accepted that the progenitor of FRB should at least involve one neutron star or magnetar. The recently discovered magnetar-associated burst in our Milky Way strongly supports the magnetar origin of some, if not all FRBs [12, 27]. The statistical similarity between repeating FRBs and soft gamma repeaters further implies that they may have similar origin [28, 29].

FRBs are energetic enough to be detectable up to high redshift, therefore they can be used as probes to investigate the cosmology [30–37], and to test the fundamental physics [38–42]. Unfortunately, up to now most FRBs have no direct measurement of redshift. Although hundreds of FRBs have been measured, only a dozen of them are well localized. With such a small sample,

Received June 1, 2023

^{*} Supported by the National Natural Science Fund of China under grant Nos. 11873001, 12147102 and 12275034.

1) E-mail: linhn@cqu.edu.cn

©2019 Chinese Physical Society and the Institute of High Energy Physics of the Chinese Academy of Sciences and the Institute of Modern Physics of the Chinese Academy of Sciences and IOP Publishing Ltd

we even do not clearly know the redshift distribution of FRBs. One way to solve this problem is to use the observed DM, which is an indicator of distance, to infer the redshift [43–46]. To this end, one should reasonably model the DM contribution from host galaxy and subtract it from the total observed DM. This is not an easy task, because too many factors may affect the host DM, such as the galaxy type, the inclination angle, the mass of host galaxy, the offset of FRB site from galaxy center, etc. A simple but rough assumption is that the host DM is a universal constant for all FRBs [31, 35, 46]. Alternatively, Luo et al. [47] assumed that the host DM follows the star-formation rate (SFR) of the host galaxy. However, Lin et al. [48] found no strong correlation between host DM and SFR from the limited sample of localized FRBs. A more reasonable way to deal with the host DM is to model it using a proper probability distribution and marginalize over the free parameters [36, 49, 50]. For example, Macquart et al. [49] assumed that the host DM follows log-normal distribution, and reconstructed the DM-redshift relation from five well-localized FRBs. However, due to the small data sample, the DM-redshift relation has large uncertainty. As the discovery of more and more FRBs in recent years, it is interesting to recheck the DM-redshift relation and use it to infer the redshift of FRBs which has no direct measurement of spectroscopic or photometric redshift.

In this paper, we assume that the host DM of FRBs follows log-normal distribution, and reconstruct the DM-redshift relation from well localized FRBs using Bayesian inference method. Then the DM-redshift relation is used to infer the redshift of the first CHIME/FRB catalog [11]. We further use the inferred redshift to calculate the isotropic energy of the CHIME/FRBs. The rest parts of this paper are arranged as follows: In Section 2, we reconstruct the DM-redshift relation from well-localized FRBs. In Section 3, we investigate the redshift and energy distributions of CHIME/FRBs. Finally, discussion and conclusions are given in Section 4.

2 The DM-redshift relation from localized FRBs

The interaction of electromagnetic waves with plasma leads to the frequency-dependent light speed. This plasma effect, although small, may cause detectable time delay between electromagnetic waves of different frequencies, if it is accumulated at cosmological distance. This phenomenon is more obvious for low-frequency electromagnetic waves, such as the radio wave as is observed in e.g. FRBs. The time delay between low- and high-frequency electromagnetic waves propagating from a distant source to earth is proportional to the integral of electron number density along the line-of-sight, i.e. the

so called dispersion measure (DM). The observed DM of an extragalactic FRB can generally be decomposed into four main parts: the Milky Way interstellar medium (DM_{MW}), the Galactic halo (DM_{halo}), the intergalactic medium (DM_{IGM}), and the host galaxy (DM_{host}) [49, 51, 52],

$$DM_{\text{obs}} = DM_{\text{MW}} + DM_{\text{halo}} + DM_{\text{IGM}} + \frac{DM_{\text{host}}}{1+z}, \quad (1)$$

where DM_{host} is the DM of host galaxy in the FRB source frame, and the factor $1+z$ arises from the cosmic expansion. Occasionally, the DM_{halo} term is ignored, but this term is comparable to, or even larger than the DM_{MW} term for FRBs at high Galactic latitude.

The Milky Way ISM term (DM_{MW}) can be well modeled from pulsar observations, such as the NE2001 model [53] and the YMW16 model [54]. For FRBs at high Galactic latitude, both models give consistent results. However, it is pointed out that the YMW16 model may overestimate DM_{MW} at low Galactic latitude [55]. Therefore, we use the NE2001 model to estimate the DM_{MW} term. The Galactic halo term (DM_{halo}) is not well constrained yet, and Prochaska & Zheng [56] estimated that it is about in the range $50 \sim 80 \text{ pc cm}^{-3}$. Here we follow Macquart et al. [49] and assume a conservative estimation on it, i.e. $DM_{\text{halo}} = 50 \text{ pc cm}^{-3}$. The concrete value of DM_{halo} should not strongly affect our results, as its uncertainty is much smaller than the uncertainties of the DM_{IGM} and DM_{host} terms described below. Therefore, the first two terms on the right-hand-side of equation (1) can be subtracted from the observed DM_{obs} . For convenience, we define the extragalactic DM as

$$DM_{\text{E}} \equiv DM_{\text{obs}} - DM_{\text{MW}} - DM_{\text{halo}} = DM_{\text{IGM}} + \frac{DM_{\text{host}}}{1+z}. \quad (2)$$

Given a specific cosmological model, the DM_{IGM} term can be calculated theoretically. Assuming that both hydrogen and helium are fully ionized [57, 58], the DM_{IGM} term can be written in the standard Λ CDM model as [43, 51]

$$\langle DM_{\text{IGM}}(z) \rangle = \frac{21cH_0\Omega_b f_{\text{IGM}}}{64\pi Gm_p} \int_0^z \frac{1+z}{\sqrt{\Omega_m(1+z)^3 + \Omega_\Lambda}} dz, \quad (3)$$

where f_{IGM} is the fraction of baryon mass in IGM, m_p is the proton mass, H_0 is the Hubble constant, G is the Newtonian gravitational constant, Ω_b is the normalized baryon matter density, Ω_m and Ω_Λ are the normalized densities of matter (including baryon matter and dark matter) and dark energy, respectively. In this paper, we work in the standard Λ CDM model with the Planck 2018 parameters, i.e. $H_0 = 67.4 \text{ km s}^{-1} \text{ Mpc}^{-1}$, $\Omega_m = 0.315$, $\Omega_\Lambda = 0.685$ and $\Omega_b = 0.0493$ [59]. The fraction of baryon mass in IGM can be tightly constrained by directly observing the budget of baryons in different states [60], or

observing the radio dispersion on gamma-ray bursts [61]. All the observations show that f_{IGM} is about 0.84. Using five well-localized FRBs, Li et al. [33] also obtained the similar result. Therefore, we fix $f_{\text{IGM}} = 0.84$ to reduce the freedom. The uncertainty of these parameters should not significantly affect our results, since they are much smaller than the variation of DM_{IGM} described below.

Note that equation (3) should be interpreted as the mean contribution from IGM. Due to the large-scale matter density fluctuation, the actual value would vary around the mean. Theoretical analysis and hydrodynamic simulations show that the probability distribution for DM_{IGM} has a flat tail at large values, which can be fitted with the following function [49, 62]

$$p_{\text{IGM}}(\Delta) = A\Delta^{-\beta} \exp\left[-\frac{(\Delta^{-\alpha} - C_0)^2}{2\alpha^2\sigma_{\text{IGM}}^2}\right], \quad \Delta > 0, \quad (4)$$

where $\Delta \equiv \text{DM}_{\text{IGM}}/\langle \text{DM}_{\text{IGM}} \rangle$, σ_{IGM} is the effective standard deviation, α and β are related to the inner density profile of gas in haloes, A is a normalization constant, and C_0 is chosen such that the mean of this distribution is unity. Hydrodynamic simulations show that $\alpha = \beta = 3$ provides the best match to the model [49, 62], thus we fix these two parameters. Simulations also show that the standard deviation σ_{IGM} approximately scales with redshift as $z^{-1/2}$ in the redshift range $z \lesssim 1$ [63, 64]. The redshift-dependence of σ_{IGM} is still unclear at $z > 1$, so we just simply extrapolate this relation to high-redshift region. Therefore, we follow Macquart et al. [49] and parameterize it as $\sigma_{\text{IGM}} = Fz^{-1/2}$, where F is a free parameter.

Due to the lack of detailed observation on the local environment of FRB source, the host term DM_{host} is poorly known. It may range from several tens to several hundreds pc cm^{-3} . For example, Xu et al. [15] estimated that the DM_{host} of the repeating burst FRB20201124A is in the range $10 < \text{DM}_{\text{host}} < 310 \text{ pc cm}^{-3}$; Niu et al. [65] inferred $\text{DM}_{\text{host}} \approx 900 \text{ pc cm}^{-3}$ for FRB20190520B. Numerical simulations show that the probability of DM_{host} follows the log-normal distribution [49, 50],

$$p_{\text{host}}(\text{DM}_{\text{host}}|\mu, \sigma_{\text{host}}) = \frac{1}{\sqrt{2\pi}\text{DM}_{\text{host}}\sigma_{\text{host}}} \times \exp\left[-\frac{(\ln\text{DM}_{\text{host}} - \mu)^2}{2\sigma_{\text{host}}^2}\right] \quad (5)$$

where μ and σ_{host} are the mean and standard deviation of $\ln\text{DM}_{\text{host}}$, respectively. This distribution has a

We first use the full 17 FRBs to constrain the free parameters $(F, e^\mu, \sigma_{\text{host}})$. We use e^μ rather than μ as a free parameter, as was done in Macquart et al. [49], because the former directly represents the median value

median value of e^μ and variance $e^{\mu+\sigma_{\text{host}}^2/2}(e^{\sigma_{\text{host}}^2} - 1)^{1/2}$. Theoretically, the log-normal distribution allows for the appearance of large value of DM_{host} , as is shown by simulations, DM_{host} may be as large as 1000 pc cm^{-3} [44]. Generally, the two parameters $(\mu, \sigma_{\text{host}})$ may be redshift-dependent, but for non-repeating bursts they do not vary significantly with redshift [50]. For simplicity, we first follow Macquart et al. [49] and treat them as two constant parameters. The possible redshift-dependence will be investigated later.

Given the distributions p_{IGM} and p_{host} , the probability distribution of DM_{E} at redshift z can be calculated as [49]

$$p_{\text{E}}(\text{DM}_{\text{E}}|z) = \int_0^{(1+z)\text{DM}_{\text{E}}} p_{\text{host}}(\text{DM}_{\text{host}}|\mu, \sigma_{\text{host}}) \times p_{\text{IGM}}(\text{DM}_{\text{E}} - \frac{\text{DM}_{\text{host}}}{1+z}|F, z) d\text{DM}_{\text{host}} \quad (6)$$

The likelihood that we observe a sample of FRBs with $\text{DM}_{\text{E},i}$ at redshift z_i ($i = 1, 2, 3, \dots, N$) is given by

$$\mathcal{L}(\text{FRBs}|F, \mu, \sigma_{\text{host}}) = \prod_{i=1}^N p_{\text{E}}(\text{DM}_{\text{E},i}|z_i), \quad (7)$$

where N is the total number of FRBs. Given the FRB data $(z_i, \text{DM}_{\text{E},i})$, the posterior probability distribution of the parameters $(F, \mu, \sigma_{\text{host}})$ is given according to Bayes theorem by

$$P(F, \mu, \sigma_{\text{host}}|\text{FRBs}) \propto \mathcal{L}(\text{FRBs}|F, \mu, \sigma_{\text{host}})P_0(F, \mu, \sigma_{\text{host}}), \quad (8)$$

where P_0 is the prior of the parameters.

Up to now, there are 19 well-localized extragalactic FRBs that have direct identification of host galaxy and well measured redshift*. Among them, we ignore FRB20200120E and FRB20190614D. The former is very close to our Galaxy (3.6 Mpc), and the peculiar velocity dominates over the Hubble flow, hence has a negative redshift $z = -0.0001$ [66, 67]. The latter has no direct measurement of spectroscopic redshift, but has a photometric redshift $z \approx 0.6$ [68]. All the rest 17 FRBs have well measured spectroscopic redshift. The main properties of the 17 FRBs are listed in Table 1, which will be used in the following to reconstruct the DM_{E} -redshift relation.

of DM_{host} . The posterior probability density functions of the free parameters are calculated using the publicly available python package `emcee` [77], while the other cosmological parameters are fixed to the Planck 2018 val-

*The FRB Host Database, <http://frbhosts.org/>

Table 1. The properties of the Host/FRB catalog. Column 1: FRB name; Columns 2 and 3: the right ascension and declination of FRB source on the sky; Column 4: the observed DM; Column 5: the DM of the Milky Way ISM calculated using the NE2001 model; Column 6: the extragalactic DM calculated by subtracting DM_{MW} and DM_{halo} from the observed DM_{obs} , assuming $DM_{\text{halo}} = 50 \text{ pc cm}^{-3}$ for the Milky Way halo; Column 7: the spectroscopic redshift; Column 8: repeating or non-repeating; Column 9: the references.

FRBs	RA [$^{\circ}$]	Dec [$^{\circ}$]	DM_{obs} [pc cm^{-3}]	DM_{MW} [pc cm^{-3}]	DM_{E} [pc cm^{-3}]	z_{sp}	repeat?	reference
20121102A	82.99	33.15	557.00	157.60	349.40	0.1927	Yes	Chatterjee et al. [8]
20180301A	93.23	4.67	536.00	136.53	349.47	0.3305	Yes	Bhandari et al. [69]
20180916B	29.50	65.72	348.80	168.73	130.07	0.0337	Yes	Marcote et al. [70]
20180924B	326.11	-40.90	362.16	41.45	270.71	0.3214	No	Bannister et al. [71]
20181030A	158.60	73.76	103.50	40.16	13.34	0.0039	Yes	Bhardwaj et al. [72]
20181112A	327.35	-52.97	589.00	41.98	497.02	0.4755	No	Prochaska et al. [73]
20190102C	322.42	-79.48	364.55	56.22	258.33	0.2913	No	Macquart et al. [49]
20190523A	207.06	72.47	760.80	36.74	674.06	0.6600	No	Ravi et al. [74]
20190608B	334.02	-7.90	340.05	37.81	252.24	0.1178	No	Macquart et al. [49]
20190611B	320.74	-79.40	332.63	56.60	226.03	0.3778	No	Macquart et al. [49]
20190711A	329.42	-80.36	592.60	55.37	487.23	0.5217	Yes	Macquart et al. [49]
20190714A	183.98	-13.02	504.13	38.00	416.13	0.2365	No	Heintz et al. [75]
20191001A	323.35	-54.75	507.90	44.22	413.68	0.2340	No	Heintz et al. [75]
20191228A	344.43	-29.59	297.50	33.75	213.75	0.2432	No	Bhandari et al. [69]
20200430A	229.71	12.38	380.25	27.35	302.90	0.1608	No	Bhandari et al. [69]
20200906A	53.50	-14.08	577.80	36.19	491.61	0.3688	No	Bhandari et al. [69]
20201124A	77.01	26.06	413.52	126.49	237.03	0.0979	Yes	Fong et al. [76]

ues [59]. The same flat priors as that in Macquart et al. [49] are used for the free parameters: $F \in \mathcal{U}(0.01, 0.5)$, $e^\mu \in \mathcal{U}(20, 200) \text{ pc cm}^{-3}$ and $\sigma_{\text{host}} \in \mathcal{U}(0.2, 2.0)$. The posterior probability density functions and the confi-

dence contours of the free parameters are plotted in the left panel of Figure 1. The median values and 1σ uncertainties of the free parameters are $F = 0.32^{+0.11}_{-0.10}$, $e^\mu = 102.02^{+37.65}_{-31.06} \text{ pc cm}^{-3}$ and $\sigma_{\text{host}} = 1.10^{+0.31}_{-0.23}$.

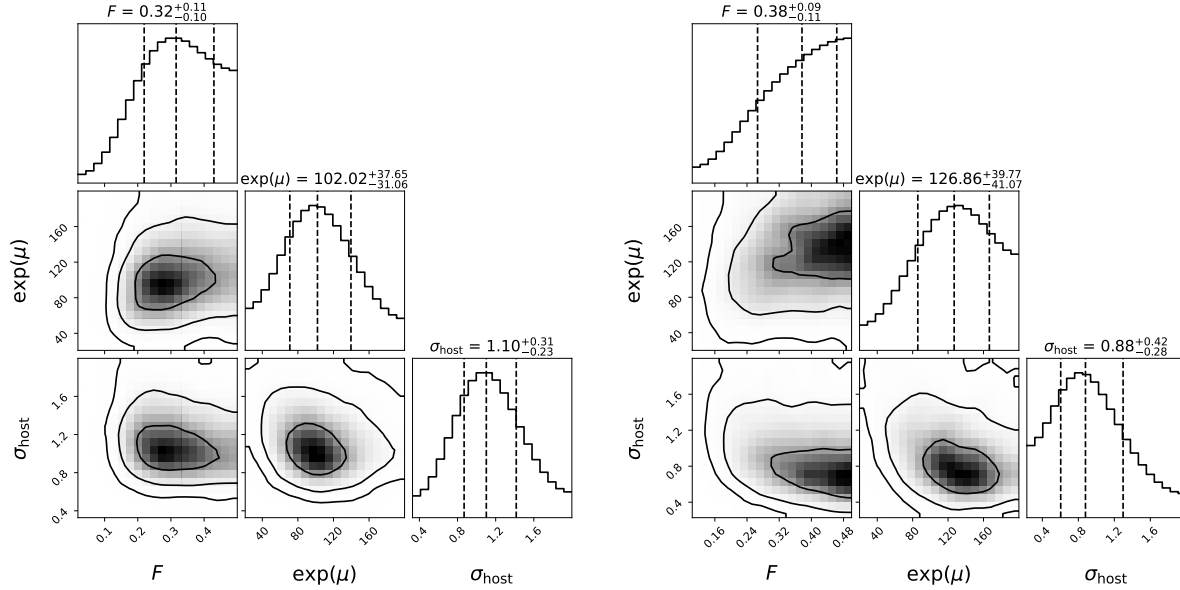


Figure 1. Constraints on the free parameters ($F, e^\mu, \sigma_{\text{host}}$) using the full sample (left panel) and the non-repeaters (right panel). The contours from the inner to outer represent 1σ , 2σ and 3σ confidence regions, respectively.

With the parameters ($F, e^\mu, \sigma_{\text{host}}$) constrained, we calculate the probability distribution of DM_{E} at any redshift in the range $0 < z < 4$ according to equation (6). The reconstructed $\text{DM}_{\text{E}}-z$ relation is plotted in the left panel of Figure 2. The dark blue line is the median value and the light blue region is the 1σ uncertainty. For comparison, we also plot the best-fitting curve by directly fitting equation (2) to the FRB data using the least- χ^2 method (the red-dashed line), where DM_{IGM} is replaced by its mean given in equation (3). The least- χ^2 method is equivalent to assume that both DM_{IGM} and DM_{host} follow Gaussian distribution around the mean. The least- χ^2 curve gradually deviates from the median value of the reconstructed $\text{DM}_{\text{E}}-z$ relation at high redshift, but due to the large uncertainty they are still consistent within 1σ uncertainty. We find that 15 out of the 17 FRBs well fall into the 1σ range of the reconstructed $\text{DM}_{\text{E}}-z$ relation. Two outliers, FRB20181030A

and FRB20190611B (the red dots in Figure 2), fall below the 1σ range of the $\text{DM}_{\text{E}}-z$ relation, imply that the DM_{E} values of these two FRBs are smaller than expected. We note that the outlier FRB20181030A has a very smaller redshift ($z = 0.0039$) and a very low extragalactic DM ($\text{DM}_{\text{E}} = 13.34 \text{ pc cm}^{-3}$), so the peculiar velocity of its host galaxy couldn't be ignored. The redshift of the other outlier FRB20190611B is $z = 0.3778$, and the observed DM of this burst is $\text{DM}_{\text{obs}} = 332.63 \text{ pc cm}^{-3}$. The normal burst FRB20200906A has a redshift ($z = 0.3688$) similar to FRB20190611B, but with a much larger DM ($\text{DM}_{\text{obs}} = 577.8 \text{ pc cm}^{-3}$). Note that both FRB20200906A and FRB20190611B are non-repeating, and the sky positions of these two bursts differ significantly. The large difference of DM_{obs} of these two bursts may be caused by e.g. the fluctuation of matter density in IGM, the variation of host DM, or different local environment of FRB source [65, 78].

The full FRB sample includes 11 non-repeating FRBs and 6 repeating FRBs. The repeaters and non-repeaters may have different DM_{host} . To check this, we re-constrain the parameters ($F, e^\mu, \sigma_{\text{host}}$) using the 11 non-

repeating FRBs. The confidence contours and the posterior probability distributions of the parameter space are plotted in the right panel of Figure 1. The median values and 1σ uncertainties of the free param-

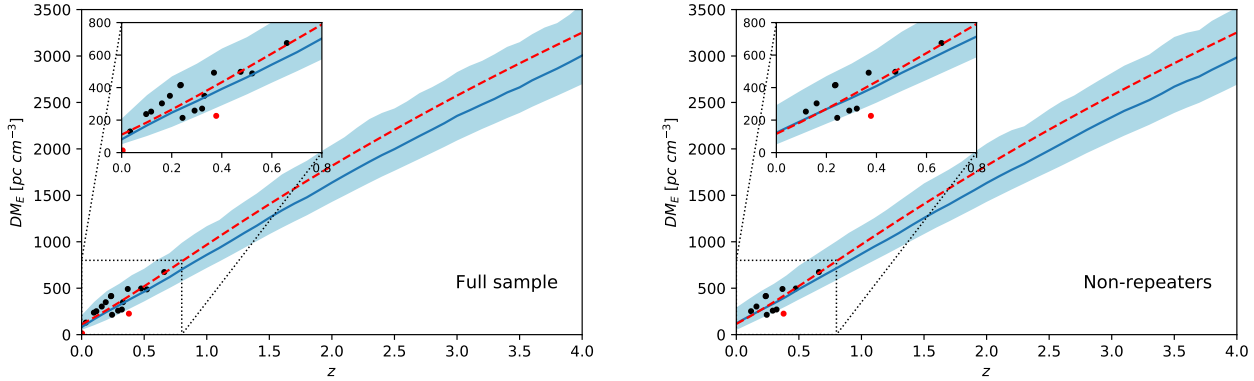


Figure 2. The $DM_E - z$ relation obtained from full sample (left panel) and non-repeaters (right panel). The dark blue line is the median value and the light blue region is 1σ uncertainty. The dots are the FRB data points and the outliers are highlighted in red. The red-dashed line is the best-fitting result obtained using the least- χ^2 method. The inset is the zoom-in of the low-redshift range.

ters are $F = 0.38^{+0.09}_{-0.11}$, $e^\mu = 126.86^{+39.77}_{-41.07}$ pc cm^{-3} and $\sigma_{\text{host}} = 0.88^{+0.42}_{-0.28}$. We obtain a little larger e^μ value but a smaller σ_{host} value than that constrained from the full FRBs. But they are still consistent with 1σ uncertainty. The reconstructed $DM_E - z$ relation using the non-repeating sample is shown in the right panel of Figure 2. FRB20190611B is still an outlier (the other outlier FRB20181030A is a repeater). The $DM_E - z$ relations of the full sample and the non-repeaters are well consistent with each other, but the latter has a little larger uncertainty, especially at the low-redshift range.

In general, e^μ and σ_{host} may evolve with redshift. Numerical simulations shows that the median value of DM_{host} has a power-law dependence on redshift, but σ_{host} does not change significantly [50]. To check this, we parameterize e^μ in the power-law form,

$$e^\mu = e^{\mu_0} (1+z)^\alpha, \quad (9)$$

and use the full FRB sample to constrain the parameters

3 The redshift and energy distribution of CHIME/FRBs

The first CHIME/FRB catalog consists of 536 bursts, including 474 apparently non-repeating bursts and 62 repeating bursts from 18 FRB sources [11]. In this paper, we focus on the 474 apparently non-repeating bursts, whose properties are listed in a long table in the *online material*. All the bursts have well measured DM_{obs} , but most of them have no direct measurement of redshift. We calculate the extragalactic DM_E by subtracting DM_{MW} and DM_{halo} from the observed DM_{obs} , where DM_{MW} is calculated using the NE2001 model [53], and DM_{halo} is assumed to be 50 pc cm^{-3} [49]. The DM_E values of the 474 apparently non-repeating bursts fall into

($F, e^{\mu_0}, \sigma_{\text{host}}, \alpha$). Flat prior is adopted for α in the range $\alpha \in \mathcal{U}(-2, 2)$. The posterior probability density functions and the confidence contours of the free parameters are plotted in the left panel of Figure 3. The best-fitting parameters are $F = 0.32^{+0.11}_{-0.10}$, $e^{\mu_0} = 98.71^{+45.75}_{-33.06}$ pc cm^{-3} , $\sigma_{\text{host}} = 1.08^{+0.32}_{-0.22}$ and $\alpha = 0.15^{+1.21}_{-1.33}$. As can be seen, the parameter α couldn't be tightly constrained, while the constraints on the other three parameters are almost unchanged compared to the case when $\alpha = 0$ fixed. This implies that there is no evidence for the redshift-dependence of e^μ with the present data. With the non-repeating FRBs, we arrive at the same conclusion (see the right panel of Figure 3). Therefore, it is safe to assume that e^μ is redshift-independent, at least in the low-redshift range $z < 1$. But be caution that the universality of e^μ has not been proven at high redshift. Hence, the uncertainty on the $DM_E - z$ relation in $z > 1$ range may be underestimated.

the range $20 - 3000 \text{ pc cm}^{-3}$. Among them 444 bursts have $DM_E > 100 \text{ pc cm}^{-3}$, while the rest 30 bursts have $DM_E < 100 \text{ pc cm}^{-3}$. The mean and median values of DM_E are 557 and 456 pc cm^{-3} , respectively. We divide the DM_E of the full non-repeating bursts into 30 uniform bins, with bin width $\Delta DM_E = 100 \text{ pc cm}^{-3}$, and plot the histogram in the left panel of Figure 4. The distribution of DM_E can be well fitted by cut-off power law (CPL),

$$\text{CPL: } N(x) \propto x^\alpha \exp\left(-\frac{x}{x_c}\right), \quad x > 0, \quad (10)$$

with the best-fitting parameters $\alpha = 0.86 \pm 0.07$ and $x_c = 289.49 \pm 17.90 \text{ pc cm}^{-3}$. This distribution has a peak at $x_p = \alpha x_c \approx 250 \text{ pc cm}^{-3}$, which is much smaller than the median value and mean value of DM_E .

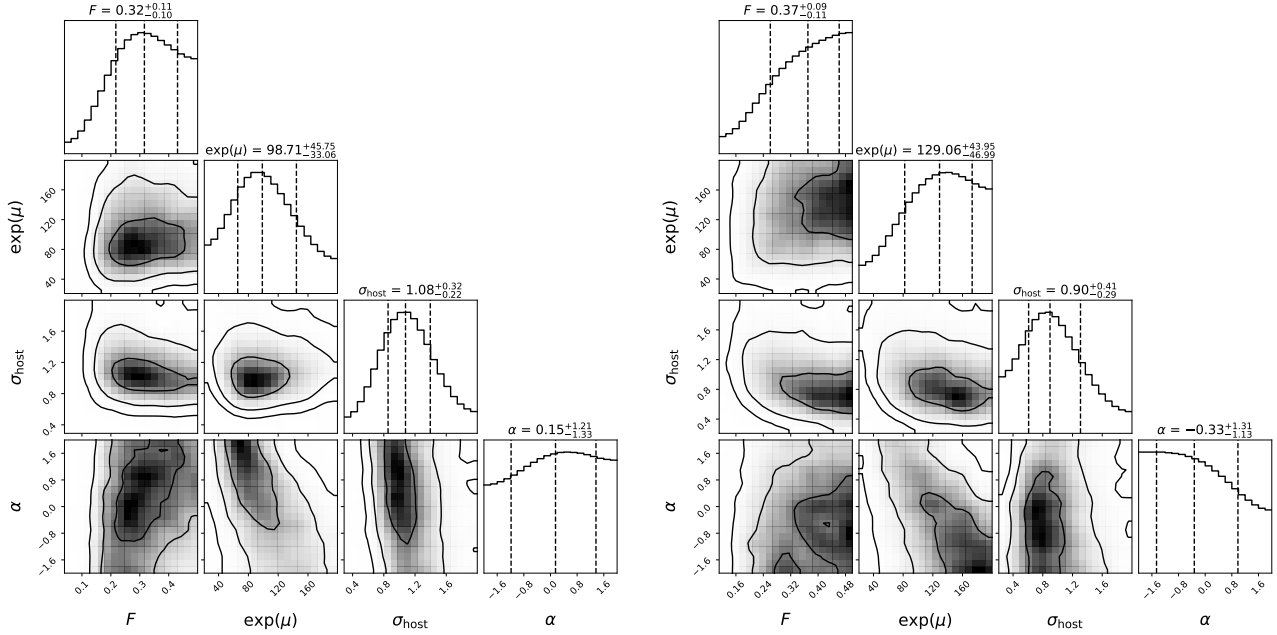


Figure 3. Constraints on the free parameters ($F, e^{\mu_0}, \sigma_{\text{host}}, \alpha$) using the full sample (left panel) and the non-repeaters (right panel). The contours from the inner to outer represent 1σ , 2σ and 3σ confidence regions, respectively.

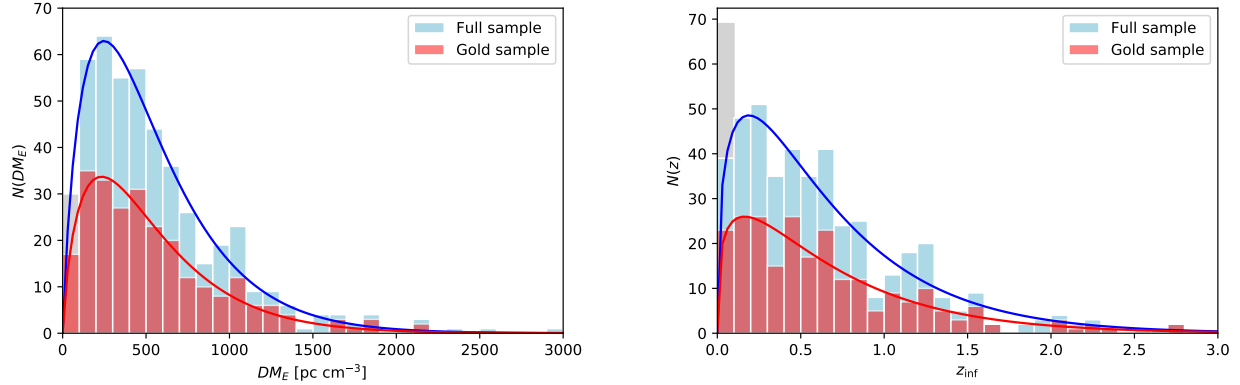


Figure 4. The histogram of DM_E (left panel) and inferred redshift (right panel) of the first non-repeating CHIME/FRB catalog. The left-most gray bar represent the 30 FRBs with $DM_E < 100 \text{ pc cm}^{-3}$, which are expected to have $z < 0.1$. The blue and red lines are the best-fitting CPL models for the Full sample and the Gold sample, respectively.

Now we use the $DM_E - z$ relation reconstructed using the full sample (using the non-repeating sample does not significantly affect our results) to infer the redshift of the non-repeating CHIME/FRBs. For FRBs with $DM_E < 100 \text{ pc cm}^{-3}$, the DM_{host} term may dominate over the DM_{IGM} term, hence a smaller uncertainty on DM_{host} may cause large bias on the estimation of redshift. Therefore, when inferring the redshift using $DM_E - z$ relation, we only consider the FRBs with $DM_E > 100 \text{ pc cm}^{-3}$. From the $DM_E - z$ relation we

can know that $DM_E(z = 0.1) = 169.9^{+196.9}_{-73.4} \text{ pc cm}^{-3}$ (1σ uncertainty). Therefore, FRBs with $DM_E < 100 \text{ pc cm}^{-3}$ are expected to have redshift $z < 0.1$, while the lower limit is unable to be determined. The inferred redshifts for FRBs with $DM_E > 100 \text{ pc cm}^{-3}$ are given in the *online material*. The inferred redshifts span the range $z_{\text{inf}} \in (0.023, 3.935)$. Three bursts have inferred redshift larger than 3, i.e., FRB20180906B with $z_{\text{inf}} = 3.935^{+0.463}_{-0.705}$, FRB20181203C with $z_{\text{inf}} = 3.003^{+0.443}_{-0.657}$, and FRB20190430B with $z_{\text{inf}} = 3.278^{+0.449}_{-0.650}$.

We divide the redshift range $0 < z < 3$ into 30 uniform bins, with bin width $\Delta z = 0.1$, and plot the histogram of the inferred redshift in the right panel of Figure 4. The distribution of the inferred redshift can be fitted by CPL model given in equation (10). The best-fitting parameters are $\alpha = 0.39 \pm 0.09$ and $x_c = 0.48 \pm 0.06$. The distribution has a peak at $z_p = \alpha x_c \approx 0.19$. The mean and median value of this distribution are 0.67 and 0.52, respectively. Considering the FRBs with $DM_E < 100 \text{ pc cm}^{-3}$ (30 FRBs in total), which are expected to have $z < 0.1$, there is a large excess compared to the CPL model in the redshift range $z < 0.1$ (see the left-most gray bar in Figure 4). This may be caused by the selection effect, since the detector is more sensitive to the near FRBs.

Amiri et al. [11] provided a set of criteria to exclude events which are unsuitable to be used in population analyses. (1) Events with $S/N < 12$ are excluded; (2) Events having $DM_{\text{obs}} < 1.5 \max(DM_{\text{NE2001}}, DM_{\text{YMW16}})$

are excluded; (3) Events detected in far sidelobes are excluded; (4) Events detected during non-nominal telescope operations are excluded; (5) Highly scattered events ($\tau_{\text{scat}} > 10 \text{ ms}$) are excluded. We call the remaining FRBs the Gold sample, which consists of 253 non-repeating FRBs. We plot the distributions of DM_E and redshifts of the Gold sample (together with the Full sample) in Figure 4. Similar to the Full sample, the distributions of DM_E and redshifts of the Gold sample can also be fitted by CPL model. The best-fitting CPL model parameters are summarized in Table 2. We see that parameters are not significantly changed compared to the Full sample. Note that the redshift distribution of the Gold sample shown in the right panel of Figure 4 only contains the FRBs with $DM_E > 100 \text{ pc cm}^{-3}$ (236 FRBs). The Gold sample still contains 17 FRBs with $DM_E < 100 \text{ pc cm}^{-3}$, whose redshifts are expected to be $z < 0.1$. So the low-redshift excess still exists in the Gold sample.

Table 2. The best-fitting CPL model parameters for the distributions of DM_E and redshift.

DM_E (Full)	$\alpha = 0.86 \pm 0.07$	$x_c = 289.49 \pm 17.90 \text{ pc cm}^{-3}$
DM_E (Gold)	$\alpha = 0.77 \pm 0.09$	$x_c = 302.82 \pm 23.92 \text{ pc cm}^{-3}$
redshift (Full)	$\alpha = 0.39 \pm 0.09$	$x_c = 0.48 \pm 0.06$
redshift (Gold)	$\alpha = 0.31 \pm 0.11$	$x_c = 0.52 \pm 0.08$

Given the redshift, the isotropic energy of a burst can be calculated as [79]

$$E = \frac{4\pi d_L^2 F \Delta\nu}{(1+z)^{2+\alpha}}, \quad (11)$$

where d_L is the luminosity distance, F is the average fluence, α is the spectral index ($F_\nu \propto \nu^\alpha$), and $\Delta\nu$ is the waveband in which the fluence is observed. The fluence listed in the first CHIME/FRB catalog is averaged over the 400–800 MHz waveband, hence $\Delta\nu = 400 \text{ MHz}$. The spectra indices of some bursts are not clear. Macquart et al. [80] showed that for a sample of ASKAP/FRBs, $\alpha = -1.5$ provides a reasonable fit. Hence, we fix $\alpha = -1.5$ for all the bursts. Note that the fluence given in

the CHIME/FRB catalog is lower limit, since the fluence is measured assuming each FRB is detected at the location of maximum sensitivity. So the energy calculated using equation (11) is lower limit. With the inferred redshift, we calculate the isotropic energy in the standard Λ CDM cosmology with the Planck 2018 parameters [59]. The uncertainty of energy propagates from the uncertainties of fluence and redshift. The results are given in the *online material*. The isotropic energy spans about five orders of magnitude, from 10^{37} erg to 10^{42} erg , with the median value $\sim 10^{40} \text{ erg}$. Three bursts have energy above 10^{42} erg , see Table 3. The isotropic energy of the furthest burst, FRB20180906B, is about $4 \times 10^{41} \text{ erg}$.

Several works show that the distributions of fluence and energy of repeating FRBs follow simple power law (SPL) [81, 82]. To check if the fluence and energy of the apparently non-repeating FRBs follow the same distribution or not, we calculate the cumulative distributions of fluence and energy of the non-repeating CHIME/FRBs (for both the Full sample and the Gold sample), and plot the results in Figure 5. We try to fit the cumulative

distributions of fluence and energy using the SPL model,

$$\text{SPL: } N(>x) \propto (x^{-\beta} - x_c^{-\beta}), \quad x < x_c, \quad (12)$$

where x_c is the cut-off value above which the FRB count is zero. The uncertainty of N is given by $\sigma_N = \sqrt{N}$ [82]. The best-fitting parameters are summarized in Table 4, and the best-fitting lines are shown in Figure 5 (the dashed lines). As can be seen, for both the Full sample and the Gold sample, the SPL model fails to fit

Table 3. The most energetic bursts with $E > 10^{42}$ erg. Column 1: FRB name; Columns 2 and 3: the right ascension and declination of FRB source on the sky; Column 4: the observed DM; Column 5: the DM of the Milky Way ISM calculated using the NE2001 model; Column 6: the extragalactic DM calculated by subtracting DM_{MW} and DM_{halo} from the observed DM_{obs} , assuming $DM_{halo} = 50 \text{ pc cm}^{-3}$ for the Milky Way halo; Column 7: the observed fluence; Column 8: the inferred redshift; Column 9: the isotropic energy; Column 10: the flag for Gold sample (flag=1) or not (flag=0). Note that the uncertainty of energy may be underestimated due to the lack of well-localized FRBs at $z > 1$.

FRBs	RA [$^{\circ}$]	Dec [$^{\circ}$]	DM_{obs} [pc/cm^3]	DM_{MW} [pc/cm^3]	DM_E [pc/cm^3]	Fluence [Jy ms]	z_{inf}	$\log(E/\text{erg})$	flag
20181219B	180.79	71.55	1950.7	35.8	1864.9	27.00 ± 22.00	$2.300^{+0.357}_{-0.511}$	$42.405^{+0.388}_{-0.962}$	1
20190228B	50.01	81.94	1125.8	81.9	993.9	66.00 ± 32.00	$1.175^{+0.205}_{-0.355}$	$42.170^{+0.324}_{-0.633}$	0
20190319A	113.43	5.72	2041.3	109.0	1882.3	19.40 ± 4.20	$2.325^{+0.359}_{-0.516}$	$42.271^{+0.214}_{-0.335}$	1

the distributions of fluence and energy. Especially at the left end, where the model prediction much exceeds the data points.

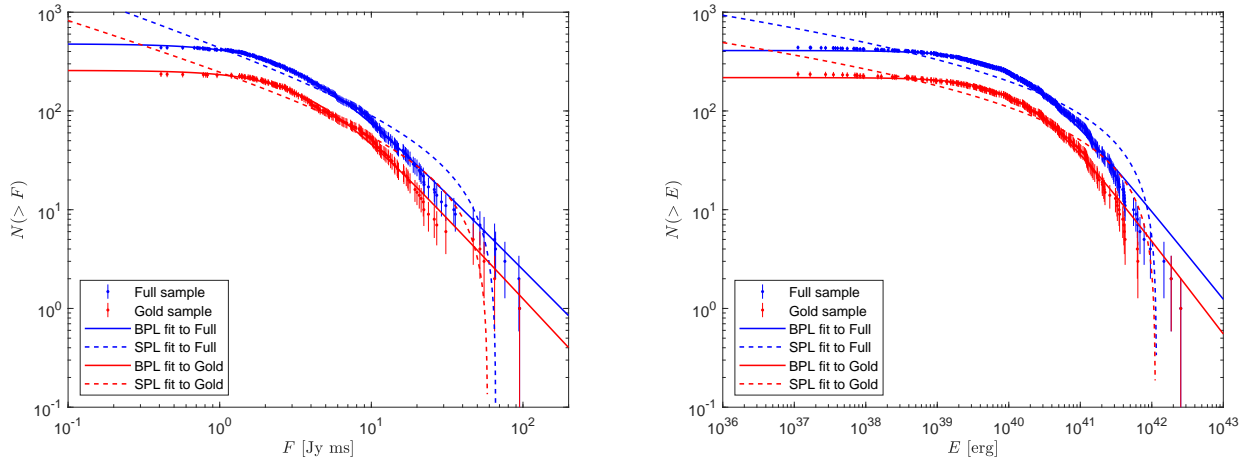


Figure 5. The cumulative distribution of fluence (left panel) and isotropic energy (right panel) of the non-repeating CHIME/FRBs with $DM_E > 100 \text{ pc cm}^{-3}$. The solid and dashed lines are the best-fitting BPL model and SPL model, respectively.

Lin & Sang [83] showed that the bent power law (BPL) model fits the distributions of fluence and energy of the repeating burst FRB121102 much better than the SPL model. The BPL model takes the form

$$\text{BPL: } N(>x) \propto \left[1 + \left(\frac{x}{x_b} \right)^\gamma \right]^{-1}, \quad x > 0, \quad (13)$$

where x_b is the median value of x , i.e. $N(x > x_b) = N(x < x_b)$. The BPL model has a flat tail at $x \ll x_b$, and behaves like SPL model at $x \gg x_b$. The BPL model was initially used to fit the power density spectra of gamma-ray bursts [84]. Then it was shown that the BPL model can well fit the distribution of fluence and energy of soft-

gamma repeaters [29, 85]. The choice of BPL model is inspired by the fact that the cumulative distributions of fluence and energy has a flat tail at the left end, as can be seen from Figure 5. We therefore try to fit the cumulative distributions of fluence and energy of CHIME/FRBs using the BPL model. The best-fitting parameters are summarized in Table 4, and the best-fitting lines are shown in Figure 5 (the solid lines). We see that the BPL model fits the data (both the Full sample and the Gold sample) much better than the SPL model. The BPL model fits the distribution of fluence very well in the full range. For the distribution of energy, the BPL model also well fits the data, except at the very high energy end.

Table 4. The best-fitting parameters of the cumulative distributions of fluence and energy for the Full sample and the Gold sample.

Fluence (Full)	SPL	$\beta = 0.54 \pm 0.02$	$x_c = 66.30 \pm 3.52$ Jy ms	$\chi^2/\text{dof} = 7.48$
	BPL	$\gamma = 1.55 \pm 0.01$	$x_b = 3.36 \pm 0.04$ Jy ms	$\chi^2/\text{dof} = 0.23$
Fluence (Gold)	SPL	$\beta = 0.48 \pm 0.03$	$x_c = 58.59 \pm 4.02$ Jy ms	$\chi^2/\text{dof} = 5.79$
	BPL	$\gamma = 1.65 \pm 0.02$	$x_b = 3.96 \pm 0.07$ Jy ms	$\chi^2/\text{dof} = 0.29$
Energy (Full)	SPL	$\beta = 0.09 \pm 0.01$	$x_c = (1.17 \pm 0.06) \times 10^{42}$ erg	$\chi^2/\text{dof} = 11.10$
	BPL	$\gamma = 0.90 \pm 0.01$	$x_b = (1.55 \pm 0.02) \times 10^{40}$ erg	$\chi^2/\text{dof} = 0.50$
Energy (Gold)	SPL	$\beta = 0.08 \pm 0.01$	$x_c = (1.13 \pm 0.09) \times 10^{42}$ erg	$\chi^2/\text{dof} = 7.12$
	BPL	$\gamma = 0.95 \pm 0.01$	$x_b = (1.82 \pm 0.04) \times 10^{40}$ erg	$\chi^2/\text{dof} = 0.29$

4 Discussion and conclusions

In this paper, we reconstructed the $\text{DM}_E - z$ relation from 17 well-localized FRBs at $z < 1$ using Bayesian inference method. The host DM was assumed to follow log-normal distribution with mean $\exp(\mu)$ and variance σ_{host} , and the variance of DM of IGM was assumed to be redshift-dependent ($\sigma_{\text{IGM}} = Fz^{-1/2}$). The free parameters were tightly constrained by 17 well-localized FRBs: $F = 0.32^{+0.11}_{-0.10}$, $\exp(\mu) = 102.02^{+37.65}_{-31.06}$ pc cm $^{-3}$ and $\sigma_{\text{host}} = 1.10^{+0.31}_{-0.23}$. These parameters are well consistent with that of Macquart et al. [49], who obtained $F = 0.31^{+0.13}_{-0.16}$, $\exp(\mu) = 68.2^{+59.6}_{-35.0}$ pc cm $^{-3}$ and $\sigma_{\text{host}} = 0.88^{+0.65}_{-0.45}$ from five well-localized FRBs. As the enlargement of FRB sample and one less free parameter (Ω_b), our constraint is more stringent than that of Macquart et al. [49]. We directly extrapolated these parameters to high redshift and reconstructed the $\text{DM}_E - z$ relation up to $z = 4$.

We further used the $\text{DM}_E - z$ relation to infer the redshift of the first CHIME/FRB catalog. We found that the extragalactic DM of the non-repeating CHIME/FRBs follows CPL distribution, with a peak at 250 pc cm $^{-3}$. The inferred redshift of the non-repeating CHIME/FRBs can also be fitted by CPL distribution, but with a significant excess at the low redshift range $0 < z < 0.1$, which may be caused by selection effect. We applied a set of criteria to exclude events which are susceptible to selection effect, as was described in Amiri et al. [11]. We found that the extragalactic DM, as well as redshift of the remaining FRBs (which we call the Gold sample) still follow CPL distribution, and the excess at low redshift still exists. We further used the inferred redshift to calculate the isotropic energy of the non-repeating CHIME/FRBs. It was found that the distributions of energy and fluence can be well fitted by BPL model, with power index $\gamma = 0.90 \pm 0.01$ and $\gamma = 1.55 \pm 0.01$ for energy and fluence, respectively. However, the SPL model fails to fit both the distributions of fluence and energy, even for the Gold sample. The statistical properties of the non-repeating CHIME/FRBs are similar to that of

the bursts from the repeating FRB source, FRB121102 [83]. The BPL model has a flat tail at low-energy (low-fluence) end, thus it predicts much less dim bursts than the SPL model. The flatness at low-energy (low-fluence) end can be explained by the observational incompleteness, since some dim bursts may missing from detection. Note that the BPL model reduces to SPL model at high energy end, $N(> E) \propto E^{-\gamma}$. The power-law index of the energy accumulative distribution is $\gamma \approx 0.9$, which corresponding to $\hat{\gamma} \approx 1.90$ for the differential distribution. Interestingly, the power-law index of the non-repeating CHIME/FRBs is similar to that of repeating bursts from the single source FRB 121102, with $\hat{\gamma} \approx 1.6 \sim 1.8$ [82].

We emphasize that the CPL distribution of redshift is not intrinsic. The intrinsic redshift distribution should take into account the selection effect of the detector. Due to the lack of well-localized FRBs, the intrinsic redshift distribution is still poorly known. Several possibilities have been discussed in literature, such as the distribution similar with gamma-ray bursts [31], a constant comoving number density with a Gaussian cutoff [86], the SFR history model [43], the modified SFR history model [87], the compact star merger model with various time delay [43]. In a recent work, Qiang et al. [46] considered several modified SFR history models and found that many of them are well consistent with the observed data of the first CHIME/FRB catalog, as long as the model parameters are chosen properly, but the simple SFR history model was fully ejected by the data. Hackstein et al. [44] have investigate three different intrinsic redshift distribution models (constant comoving density model, SFR history model, and stellar mass density model). After considering the selection effects of CHIME telescope, they showed that the distribution of the observed redshift should have CPL shape. It remains to be a future work to study which model fits the CHIME/FRB best. In addition, Shin et al. [88] have studied the FRB population by assuming a Schechter luminosity function, and after calibrating the selection effects, they also found that the distribution of redshift has CPL shape.

When reconstructing the $\text{DM}_E - z$ relation, it is im-

portant to reasonably deal with the DM_{host} term. The simplest way is to assume that DM_{host} is a constant [31, 35, 46]. Of course, this is inappropriate because the actual value can vary significantly from bursts to bursts. Luo et al. [47] parameterized DM_{host} as a function of SFR. However, statistical analysis of the well-localized FRBs shown that there is not strong correlation between DM_{host} and the host galaxy properties, including SFR [48]. Because there is a lack of direct observation on DM_{host} , at present the most reasonable way is to model it using a probability distribution. Theoretical analysis and numerical simulations show that the probability of DM_{host} can be modeled by log-normal distribution with mean value μ and deviation σ_{host} [49, 50]. Based on the IllustrisTNG simulation, Zhang et al. [50] showed that $\exp(\mu)$ has a power-law dependence on redshift, and the power-law index for repeating and non-repeating FRBs is slightly different. However, we found no evidence for the redshift evolution of $\exp(\mu)$ here. The median value of DM_{host} for the well localized FRBs we obtained here is about $\exp(\mu) \sim 100 \text{ pc cm}^{-3}$. It is consistent with the DM_{host} of FRB20190608B ($\sim 137 \pm 43 \text{ pc cm}^{-3}$) obtained from optical/UV observations [89].

Due to the lack of high-redshift FRBs, the uncertainty on the $DM_E - z$ relation is large at high redshift. The uncertainty mainly comes from the uncertainties on DM_{IGM} and DM_{host} . The uncertainty on DM_{IGM} at redshift $z = 1$ is about $\delta DM_{\text{IGM}} \approx 0.3 DM_{\text{IGM}} \approx 270 \text{ pc cm}^{-3}$. From the lognormal distribution, the uncertainty of DM_{host} is estimated to be $\delta DM_{\text{host}} = \exp(\mu + \sigma_{\text{host}}/2)(\exp(\sigma_{\text{host}}^2) - 1)^{1/2} \approx 200 \text{ pc cm}^{-3}$, where $\exp(\mu) \approx 100 \text{ pc cm}^{-3}$ and $\sigma_{\text{host}} \approx 1$. The uncertainties of DM_{MW} and DM_{halo} is expected to be much smaller than that of DM_{IGM} and DM_{host} , thus they have been ignored. We also ignored the DM of the FRB source, which is hard to model due the lack of knowledge on the local environment of FRBs. With the present knowledge we do not clearly know the probability distribution of DM_{source} . In some models involving the merger of compact binary, this term is expected to be small [90, 91]. Therefore, in most work this term is directly neglected. If DM_{source} does not strongly vary from burst to burst (such

that it can be treated approximately as a constant), it can be absorbed into the DM_{host} term, while the probability distribution p_{host} does not change except for an overall shift. In this case, the parameter $\exp(\mu)$ should be explained as the median value of the sum of DM_{host} and DM_{source} . Therefore, if DM_{source} does not vary significantly, including it or not should not affect our results. Another uncertainty comes from the parameter f_{IGM} . In general case, f_{IGM} should be treated as a free parameter, together with F , $\exp(\mu)$ and σ_{host} . But due to the small FRB sample, free f_{IGM} will lead to unreasonable result. So we fix $f_{\text{IGM}} = 0.84$ based on other independent observations. This will lead to the underestimation on the uncertainty of $DM_E - z$ relation.

The conclusions of our paper are based on the assumption that the $DM_E - z$ relation obtained from low-redshift data can be extrapolated to high redshift region. As is demonstrated in section 2, there is no strong evidence for the redshift dependence of host DM, at least at low-redshift region $z \lesssim 1$. But we can't prove this assumption at high redshift region, since there is lack of data points at $z > 1$. So we just simply extrapolate the $DM_E - z$ relation to high redshift region without proving it. Recent works [79, 87] show that the $DM_E - z$ relation may be nonmonotonic, with a turn point at a certain redshift. This is because that a FRB at low redshift is easier to be detected than at high redshift, for a given intrinsic luminosity. Therefore, a highly dispersed FRB is mainly caused by large DM of host galaxy, rather than by high redshift. For example, the large DM of FRB20190520B ($DM_{\text{obs}} \approx 1200 \text{ pc cm}^{-3}$, $z \approx 0.241$) main attributes to the large value of DM_{host} ($\approx 900 \text{ pc cm}^{-3}$) [65]. Therefore, the uncertainty of $DM_E - z$ relation we obtained in our paper may be significantly underestimated. We hope that the uncertainty can be reduced if more high-redshift FRBs are detected in the future.

Online material

The parameters of the first (non-repeating) CHIME/FRB catalog are listed in a long table in the online material.

References

- 1 E. Petroff, J. W. T. Hessels, D. R. Lorimer, Fast Radio Bursts, *Astron. Astrophys. Rev.* 27 (1) (2019) 4.
- 2 J. M. Cordes, S. Chatterjee, Fast Radio Bursts: An Extragalactic Enigma, *Ann. Rev. Astron. Astrophys.* 57 (2019) 417–465.
- 3 B. Zhang, The Physical Mechanisms of Fast Radio Bursts, *Nature* 587 (2020) 45–53.
- 4 D. Xiao, F. Wang, Z. Dai, The Physics of Fast Radio Bursts, *Sci. China Phys. Mech. Astron.* 64 (4) (2021) 249501.
- 5 D. R. Lorimer, M. Bailes, M. A. McLaughlin, D. J. Narkevic, F. Crawford, A bright millisecond radio burst of extragalactic origin, *Science* 318 (2007) 777.
- 6 D. Thornton, et al., A Population of Fast Radio Bursts at Cosmological Distances, *Science* 341 (6141) (2013) 53–56.
- 7 E. F. Keane, et al., A Fast Radio Burst Host Galaxy, *Nature* 530 (2016) 453–456.
- 8 S. Chatterjee, et al., The direct localization of a fast radio burst and its host, *Nature* 541 (2017) 58.
- 9 S. P. Tendulkar, et al., The Host Galaxy and Redshift of the Repeating Fast Radio Burst FRB 121102, *Astrophys. J. Lett.* 834 (2) (2017) L7.
- 10 E. Petroff, E. D. Barr, A. Jameson, E. F. Keane, M. Bailes,

- M. Kramer, V. Morello, D. Tabbara, W. van Straten, FRBCAT: The Fast Radio Burst Catalogue, *Publ. Astron. Soc. Austral.* 33 (2016) e045.
- 11 M. Amiri, et al., The First CHIME/FRB Fast Radio Burst Catalog, *Astrophys. J. Supp.* 257 (2) (2021) 59.
 - 12 B. C. Andersen, et al., A bright millisecond-duration radio burst from a Galactic magnetar, *Nature* 587 (7832) (2020) 54–58.
 - 13 B. C. Andersen, et al., CHIME/FRB Discovery of Eight New Repeating Fast Radio Burst Sources, *Astrophys. J. Lett.* 885 (1) (2019) L24.
 - 14 D. Li, et al., A bimodal burst energy distribution of a repeating fast radio burst source, *Nature* 598 (7880) (2021) 267–271.
 - 15 H. Xu, et al., A fast radio burst source at a complex magnetised site in a barred galaxy, arXiv:2111.11764.
 - 16 M. Lyutikov, L. Burzawa, S. B. Popov, Fast radio bursts as giant pulses from young rapidly rotating pulsars, *Mon. Not. Roy. Astron. Soc.* 462 (1) (2016) 941–950.
 - 17 C. M. F. Mingarelli, J. Levin, T. J. W. Lazio, Fast Radio Bursts and Radio Transients from Black Hole Batteries, *Astrophys. J. Lett.* 814 (2) (2015) L20.
 - 18 B. Zhang, A “Cosmic Comb” Model of Fast Radio Bursts, *Astrophys. J. Lett.* 836 (2) (2017) L32.
 - 19 T. Totani, Cosmological Fast Radio Bursts from Binary Neutron Star Mergers, *Publ. Astron. Soc. Jpn.* 65 (2013) L12.
 - 20 J.-S. Wang, Y.-P. Yang, X.-F. Wu, Z.-G. Dai, F.-Y. Wang, Fast Radio Bursts from the Inspiral of Double Neutron Stars, *Astrophys. J. Lett.* 822 (1) (2016) L7.
 - 21 W.-M. Gu, Y.-Z. Dong, T. Liu, R. Ma, J. Wang, A Neutron Star–white Dwarf Binary Model for Repeating Fast Radio Burst 121102, *Astrophys. J. Lett.* 823 (2) (2016) L28.
 - 22 Y. F. Huang, J. J. Geng, Collision between Neutron Stars and Asteroids as a Mechanism for Fast Radio Bursts, *ASP Conf. Ser.* 502 (2016) 1.
 - 23 Z. G. Dai, J. S. Wang, X. F. Wu, Y. F. Huang, Repeating Fast Radio Bursts from Highly Magnetized Pulsars Travelling through Asteroid Belts, *Astrophys. J.* 829 (1) (2016) 27.
 - 24 Z.-N. Liu, W.-Y. Wang, Y.-P. Yang, Z.-G. Dai, Repeating Fast Radio Bursts from Pulsar–Asteroid Belt Collisions: Frequency Drifting and Polarization, *Astrophys. J.* 905 (2) (2020) 140.
 - 25 A. G. Suvorov, K. D. Kokkotas, Young magnetars with fracturing crusts as fast radio burst repeaters, *Mon. Not. Roy. Astron. Soc.* 488 (4) (2019) 5887–5897.
 - 26 J. H. Buckley, P. S. B. Dev, F. Ferrer, F. P. Huang, Fast radio bursts from axion stars moving through pulsar magnetospheres, *Phys. Rev. D* 103 (4) (2021) 043015.
 - 27 C. D. Bochenek, V. Ravi, K. V. Belov, G. Hallinan, J. Kocz, S. R. Kulkarni, D. L. McKenna, A fast radio burst associated with a Galactic magnetar, *Nature* 587 (7832) (2020) 59–62.
 - 28 J.-J. Wei, X.-F. Wu, Z.-G. Dai, F.-Y. Wang, P. Wang, D. Li, B. Zhang, Similar Scale-invariant Behaviors between Soft Gamma-Ray Repeaters and an Extreme Epoch from FRB 121102, *Astrophys. J.* 920 (2) (2021) 153.
 - 29 Y. Sang, H.-N. Lin, Statistical similarity between soft gamma repeaters and repeating fast radio bursts, *Mon. Not. Roy. Astron. Soc.* 510 (2) (2022) 1801–1808.
 - 30 J. B. Muñoz, E. D. Kovetz, L. Dai, M. Kamionkowski, Lensing of Fast Radio Bursts as a Probe of Compact Dark Matter, *Phys. Rev. Lett.* 117 (9) (2016) 091301.
 - 31 H. Yu, F. Y. Wang, Measuring the cosmic proper distance from fast radio bursts, *Astron. Astrophys.* 606 (2017) A3.
 - 32 Z.-X. Li, H. Gao, X.-H. Ding, G.-J. Wang, B. Zhang, Strongly lensed repeating fast radio bursts as precision probes of the universe, *Nature Commun.* 9 (1) (2018) 3833.
 - 33 Z. Li, H. Gao, J.-J. Wei, Y.-P. Yang, B. Zhang, Z.-H. Zhu, Cosmology-insensitive estimate of IGM baryon mass fraction from five localized fast radio bursts, *Mon. Not. Roy. Astron. Soc.* 496 (1) (2020) L28–L32.
 - 34 D.-C. Qiang, H.-K. Deng, H. Wei, Cosmic Anisotropy and Fast Radio Bursts, *Class. Quant. Grav.* 37 (18) (2020) 185022.
 - 35 Q. Wu, H. Yu, F. Y. Wang, A New Method to Measure Hubble Parameter $H(z)$ using Fast Radio Bursts, *Astrophys. J.* 895 (1) (2020) 33.
 - 36 Q. Wu, G. Q. Zhang, F. Y. Wang, An 8% Determination of the Hubble Constant from localized Fast Radio Bursts, arXiv:2108.00581.
 - 37 H.-N. Lin, Y. Sang, Probing the anisotropic distribution of baryon matter in the Universe using fast radio bursts *, *Chin. Phys. C* 45 (12) (2021) 125101.
 - 38 J.-J. Wei, H. Gao, X.-F. Wu, P. Mészáros, Testing Einstein’s Equivalence Principle With Fast Radio Bursts, *Phys. Rev. Lett.* 115 (26) (2015) 261101.
 - 39 X.-F. Wu, S.-B. Zhang, H. Gao, J.-J. Wei, Y.-C. Zou, W.-H. Lei, B. Zhang, Z.-G. Dai, P. Mészáros, Constraints on the Photon Mass with Fast Radio Bursts, *Astrophys. J. Lett.* 822 (1) (2016) L15.
 - 40 S. J. Tingay, D. L. Kaplan, Limits on Einstein’s Equivalence Principle From the First Localized Fast Radio Burst frb 150418, *Astrophys. J. Lett.* 820 (2) (2016) L31.
 - 41 L. Bonetti, J. Ellis, N. E. Mavromatos, A. S. Sakharov, E. K. G. Sarkisyan-Grinbaum, A. D. A. M. Spallicci, Photon Mass Limits from Fast Radio Bursts, *Phys. Lett. B* 757 (2016) 548–552.
 - 42 J.-J. Wei, X.-F. Wu, Testing fundamental physics with astrophysical transients, *Front. Phys.* 16 (4) (2021) 44300.
 - 43 R. C. Zhang, B. Zhang, Y. Li, D. R. Lorimer, On the energy and redshift distributions of fast radio bursts, *Mon. Not. Roy. Astron. Soc.* 501 (1) (2021) 157–167.
 - 44 S. Hackstein, M. Brüggen, F. Vazza, L. F. S. Rodrigues, Redshift estimates for fast radio bursts and implications on intergalactic magnetic fields, *Mon. Not. Roy. Astron. Soc.* 498 (4) (2020) 4811–4829.
 - 45 S. Hackstein, M. Brüggen, F. Vazza, Joint inference on the redshift distribution of fast radio burst and on the intergalactic baryon content, *Mon. Not. Roy. Astron. Soc.* 501 (3) (2021) 3825–3832.
 - 46 D.-C. Qiang, S.-L. Li, H. Wei, Fast radio burst distributions consistent with the first CHIME/FRB catalog, *JCAP* 01 (2022) 040.
 - 47 R. Luo, K. Lee, D. R. Lorimer, B. Zhang, On the normalized FRB luminosity function, *Mon. Not. Roy. Astron. Soc.* 481 (2) (2018) 2320–2337.
 - 48 H.-N. Lin, X. Li, L. Tang, Search for the correlations between host properties and DM_{host} of fast radio bursts: constraints on the baryon mass fraction in IGM, arXiv:2203.09139.
 - 49 J. P. Macquart, et al., A census of baryons in the Universe from localized fast radio bursts, *Nature* 581 (7809) (2020) 391–395.
 - 50 G. Q. Zhang, H. Yu, J. H. He, F. Y. Wang, Dispersion measures of fast radio burst host galaxies derived from IllustrisTNG simulation, *Astrophys. J.* 900 (2) (2020) 170.
 - 51 W. Deng, B. Zhang, Cosmological Implications of Fast Radio Burst/Gamma-Ray Burst Associations, *Astrophys. J. Lett.* 783 (2014) L35.
 - 52 H. Gao, Z. Li, B. Zhang, Fast Radio Burst/Gamma-Ray Burst Cosmography, *Astrophys. J.* 788 (2014) 189.
 - 53 J. M. Cordes, T. J. W. Lazio, NE2001. 1. A New model for the galactic distribution of free electrons and its fluctuations, arXiv: astro-ph/0207156.
URL <https://doi.org/10.3847/1538-4357/835/1/29>
 - 54 J. M. Yao, R. N. Manchester, N. Wang, A new electron-density model for estimation of pulsar and frb distances, *The Astrophysical Journal* 835 (1) (2017) 29. <https://doi.org/10.3847/1538-4357/835/1/29>
 - 55 S. Koch Ocker, J. M. Cordes, S. Chatterjee, Constraining Galaxy Halos from the Dispersion and Scattering of Fast Radio Bursts and Pulsars, *Astrophys. J.* 911 (2) (2021) 102.
 - 56 J. X. Prochaska, Y. Zheng, Probing Galactic haloes with fast

- radio bursts, *mnras* 485 (1) (2019) 648–665.
- 57 A. A. Meiksin, The Physics of the Intergalactic Medium, *Rev. Mod. Phys.* 81 (2009) 1405–1469.
- 58 G. D. Becker, J. S. Bolton, M. G. Haehnelt, W. L. W. Sargent, Detection of Extended He II Reionization in the Temperature Evolution of the Intergalactic Medium, *Mon. Not. Roy. Astron. Soc.* 410 (2011) 1096.
- 59 N. Aghanim, et al., Planck 2018 results. VI. Cosmological parameters, *Astron. Astrophys.* 641 (2020) A6.
- 60 M. Fukugita, C. J. Hogan, P. J. E. Peebles, The Cosmic baryon budget, *Astrophys. J.* 503 (1998) 518.
- 61 S. Inoue, Probing the cosmic reionization history and local environment of gamma-ray bursts through radio dispersion, *Mon. Not. Roy. Astron. Soc.* 348 (2004) 999.
- 62 Z. J. Zhang, K. Yan, C. M. Li, G. Q. Zhang, F. Y. Wang, Intergalactic medium dispersion measures of fast radio bursts estimated from IllustrisTNG simulation and their cosmological applications, *Astrophys. J.* 906 (1) (2021) 49.
- 63 M. McQuinn, Locating the “missing” baryons with extragalactic dispersion measure estimates, *Astrophys. J. Lett.* 780 (2014) L33.
- 64 M. Jaroszynski, Fast Radio Bursts and cosmological tests, *Mon. Not. Roy. Astron. Soc.* 484 (2) (2019) 1637–1644.
- 65 C. H. Niu, et al., A repeating fast radio burst associated with a persistent radio source, *Nature* 606 (7916) (2022) 873–877.
- 66 M. Bhardwaj, et al., A Nearby Repeating Fast Radio Burst in the Direction of M81, *Astrophys. J. Lett.* 910 (2) (2021) L18.
- 67 F. Kirsten, et al., A repeating fast radio burst source in a globular cluster, *Nature* 602 (7898) (2022) 585–589.
- 68 C. J. Law, et al., A Distant Fast Radio Burst Associated with Its Host Galaxy by the Very Large Array, *Astrophys. J.* 899 (2) (2020) 161.
- 69 S. Bhandari, et al., Characterizing the Fast Radio Burst Host Galaxy Population and its Connection to Transients in the Local and Extragalactic Universe, *Astron. J.* 163 (2) (2022) 69.
- 70 B. Marcote, et al., A repeating fast radio burst source localized to a nearby spiral galaxy, *Nature* 577 (7789) (2020) 190–194.
- 71 K. W. Bannister, et al., A single fast radio burst localized to a massive galaxy at cosmological distance, *Science* 365 (2019) 565–570.
- 72 M. Bhardwaj, et al., A Local Universe Host for the Repeating Fast Radio Burst FRB 20181030A, *Astrophys. J. Lett.* 919 (2) (2021) L24.
- 73 J. X. Prochaska, J.-P. Macquart, M. McQuinn, S. Simha, R. M. Shannon, C. K. Day, L. Marnoch, S. Ryder, A. Deller, K. W. Bannister, S. Bhandari, R. Bordoloi, J. Bunton, H. Cho, C. Flynn, E. K. Mahony, C. Phillips, H. Qiu, N. Tejos, The low density and magnetization of a massive galaxy halo exposed by a fast radio burst, *Science* 366 (6462) (2019) 231–234.
- 74 V. Ravi, et al., A fast radio burst localized to a massive galaxy, *Nature* 572 (7769) (2019) 352–354.
- 75 K. E. Heintz, J. X. Prochaska, S. Simha, E. Platts, W.-f. Fong, N. Tejos, S. D. Ryder, K. Aggerwal, S. Bhandari, C. K. Day, A. T. Deller, C. D. Kilpatrick, C. J. Law, J.-P. Macquart, A. Mannings, L. J. Marnoch, E. M. Sadler, R. M. Shannon, Host Galaxy Properties and Offset Distributions of Fast Radio Bursts: Implications for Their Progenitors, *apj* 903 (2) (2020) 152.
- 76 W.-f. Fong, et al., Chronicling the Host Galaxy Properties of the Remarkable Repeating FRB 20201124A, *Astrophys. J. Lett.* 919 (2) (2021) L23.
- 77 D. Foreman-Mackey, D. W. Hogg, D. Lang, J. Goodman, emcee: The MCMC Hammer, *Publ. Astron. Soc. Pac.* 125 (2013) 306–312.
- 78 F. Y. Wang, G. Q. Zhang, Z. G. Dai, K. S. Cheng, Repeating fast radio burst 20201124A originates from a magnetar/Be star binary, *Nature Communications* 13 (2022) 4382.
- 79 C. W. James, J. X. Prochaska, J. P. Macquart, F. O. North-Hickey, K. W. Bannister, A. Dunning, The z -DM distribution of fast radio bursts, *Mon. Not. Roy. Astron. Soc.* 509 (4) (2021) 4775–4802.
- 80 J. P. Macquart, R. M. Shannon, K. W. Bannister, C. W. James, R. D. Ekers, J. D. Bunton, The Spectral Properties of the Bright Fast Radio Burst Population, *Astrophys. J. Lett.* 872 (2) (2019) L19.
- 81 F. Y. Wang, H. Yu, SGR-like behaviour of the repeating FRB 121102, *JCAP* 03 (2017) 023.
- 82 F. Y. Wang, G. Q. Zhang, A universal energy distribution for FRB 121102, *apj* 882 (2) (2019) 108.
- 83 H.-N. Lin, Y. Sang, Scale-invariance in the repeating fast radio burst 121102, *Mon. Not. Roy. Astron. Soc.* 491 (2) (2020) 2156–2161.
- 84 C. Guidorzi, S. Dichiara, L. Amati, Individual power density spectra of Swift gamma-ray bursts, *Astron. Astrophys.* 589 (2016) A98.
- 85 Z. Chang, H.-N. Lin, Y. Sang, P. Wang, Scale-invariance in soft gamma repeaters, *Chin. Phys. C* 41 (6) (2017) 065104.
- 86 Z. Li, H. Gao, J.-J. Wei, Y.-P. Yang, B. Zhang, Z.-H. Zhu, Cosmology-independent estimate of the fraction of baryon mass in the IGM from fast radio burst observations, *Astrophys. J.* 876 (2) (2019) 146.
- 87 C. W. James, J. X. Prochaska, J. P. Macquart, F. O. North-Hickey, K. W. Bannister, A. Dunning, The fast radio burst population evolves, consistent with the star formation rate, *Mon. Not. Roy. Astron. Soc.* 510 (1) (2022) L18–L23.
- 88 K. Shin, et al., Inferring the Energy and Distance Distributions of Fast Radio Bursts Using the First CHIME/FRB Catalog, *Astrophys. J.* 944 (1) (2023) 105.
- 89 J. S. Chittidi, S. Simha, A. Mannings, J. X. Prochaska, M. Rafelski, M. Neeleman, J.-P. Macquart, N. Tejos, R. A. Jorgenson, S. D. Ryder, C. K. Day, L. Marnoch, S. Bhandari, A. T. Deller, H. Qiu, K. W. Bannister, R. M. Shannon, K. E. Heintz, Dissecting the Local Environment of FRB 190608 in the Spiral Arm of its Host Galaxy, *apj* 922 (2) (2021) 173.
- 90 B. Margalit, E. Berger, B. D. Metzger, Fast Radio Bursts from Magnetars Born in Binary Neutron Star Mergers and Accretion Induced Collapse, *apj* 886 (2) (2019) 110.
- 91 F. Y. Wang, Y. Y. Wang, Y.-P. Yang, Y. W. Yu, Z. Y. Zuo, Z. G. Dai, Fast radio bursts from activities of neutron stars newborn in BNS mergers: offset, birth rate and observational properties, *apj* 891 (1) (2020) 72.

Online Material for “Inferring redshift and energy distributions of fast radio bursts from the first CHIME/FRB catalog”

The parameters of the first (non-repeating) CHIME/FRB catalog are listed in Table 5 [The CHIME/FRB Collaboration, ApJS 257:59 (2021)]. Column 1: FRB name; Columns 2 and 3: the right ascension and declination of FRB source on the sky; Column 4: the observed DM; Column 5: the DM of the Milky Way ISM calculated using the NE2001 model; Column 6: the extragalactic DM calculated by subtracting DM_{MW} and DM_{halo} from the observed DM_{obs} , assuming $DM_{\text{halo}} = 50 \text{ pc cm}^{-3}$ for the Milky Way halo; Column 7: the observed fluence; Column 8: the inferred redshift; Column 9: the isotropic energy; Column 10: the flag for Gold sample (flag=1) or not (flag=0). The redshift and energy are only calculated for FRBs with $DM_{\text{E}} > 100 \text{ pc cm}^{-3}$. Note that the fluence and energy are the lower limits, since the fluence is measured assuming each FRB is detected at the location of maximum sensitivity.

Table 5: The parameters of the first CHIME/FRB catalog.

FRBs	RA [$^{\circ}$]	Dec [$^{\circ}$]	DM_{obs} [pc/cm^3]	DM_{MW} [pc/cm^3]	DM_{E} [pc/cm^3]	Fluence [Jy ms]	z_{inf}	$\log(E/\text{erg})$	flag
20180725A	93.42	67.07	716.6	72.4	594.2	4.10 ± 2.30	$0.668_{-0.315}^{+0.163}$	$40.418_{-0.973}^{+0.404}$	0
20180727A	197.72	26.42	642.1	21.2	570.9	2.31 ± 0.76	$0.641_{-0.340}^{+0.159}$	$40.129_{-0.900}^{+0.338}$	0
20180729A	199.40	55.58	108.4	29.6	28.8	17.00 ± 10.00	—	—	0
20180729B	89.93	56.50	318.6	95.4	173.2	1.20 ± 0.74	$0.104_{-0.081}^{+0.118}$	$38.136_{-1.737}^{+0.906}$	0
20180730A	57.39	87.19	849.2	59.5	739.7	27.00 ± 12.00	$0.848_{-0.332}^{+0.183}$	$41.468_{-0.737}^{+0.348}$	0
20180801A	322.53	72.72	656.7	91.1	515.6	7.90 ± 4.80	$0.570_{-0.313}^{+0.149}$	$40.549_{-1.171}^{+0.431}$	0
20180806A	228.56	75.62	739.2	39.9	649.3	7.60 ± 6.60	$0.736_{-0.306}^{+0.167}$	$40.780_{-1.401}^{+0.469}$	0
20180810A	101.47	34.86	415.7	105.5	260.2	1.70 ± 1.00	$0.224_{-0.166}^{+0.132}$	$38.990_{-1.617}^{+0.640}$	0
20180810B	180.41	83.14	169.8	46.5	73.3	7.90 ± 2.10	—	—	0
20180812A	19.33	80.78	795.8	73.7	672.1	5.40 ± 2.80	$0.766_{-0.317}^{+0.169}$	$40.671_{-0.834}^{+0.374}$	0
20180814B	238.26	74.02	237.8	40.6	147.2	10.60 ± 8.30	$0.075_{-0.061}^{+0.108}$	$38.780_{-2.179}^{+1.067}$	0
20180817A	233.20	42.20	1002.8	23.7	929.1	29.00 ± 16.00	$1.095_{-0.344}^{+0.198}$	$41.745_{-0.712}^{+0.349}$	0
20180904A	286.58	81.22	360.7	55.0	255.7	6.00 ± 3.40	$0.218_{-0.162}^{+0.130}$	$39.513_{-1.598}^{+0.638}$	1
20180906A	141.48	14.29	383.3	43.3	290.0	2.70 ± 1.50	$0.261_{-0.191}^{+0.142}$	$39.336_{-1.564}^{+0.606}$	0
20180906B	185.75	56.42	3037.7	31.0	2956.7	1.50 ± 0.88	$3.935_{-0.705}^{+0.463}$	$41.622_{-0.554}^{+0.295}$	0
20180907A	320.87	29.46	875.1	89.9	735.2	2.80 ± 1.40	$0.843_{-0.336}^{+0.182}$	$40.478_{-0.793}^{+0.364}$	1
20180907B	4.49	19.17	658.3	38.2	570.1	2.90 ± 1.60	$0.640_{-0.340}^{+0.159}$	$40.227_{-1.076}^{+0.405}$	1
20180907C	41.72	77.07	638.9	92.1	496.8	1.48 ± 0.69	$0.541_{-0.300}^{+0.151}$	$39.773_{-1.045}^{+0.404}$	0
20180907D	328.95	89.22	1444.4	53.3	1341.1	4.90 ± 2.30	$1.594_{-0.385}^{+0.285}$	$41.327_{-0.536}^{+0.319}$	1
20180907E	167.88	47.09	381.7	28.8	302.9	6.90 ± 3.70	$0.277_{-0.203}^{+0.144}$	$39.800_{-1.539}^{+0.585}$	1
20180909A	123.63	56.76	407.6	48.8	308.8	1.02 ± 0.41	$0.285_{-0.208}^{+0.144}$	$38.995_{-1.426}^{+0.538}$	0
20180910A	352.77	88.21	684.2	57.9	576.3	5.60 ± 3.00	$0.647_{-0.334}^{+0.160}$	$40.523_{-1.032}^{+0.400}$	1
20180911A	99.55	84.62	221.6	56.9	114.7	2.60 ± 1.90	$0.038_{-0.038}^{+0.091}$	$37.576_{-4.165}^{+1.333}$	0
20180915A	280.55	17.91	370.4	171.3	149.1	6.20 ± 3.20	$0.077_{-0.063}^{+0.109}$	$38.572_{-1.808}^{+0.987}$	1
20180915B	225.23	25.02	176.3	21.6	104.7	3.80 ± 1.00	$0.027_{-0.026}^{+0.086}$	$37.437_{-3.013}^{+1.378}$	1
20180916A	348.97	80.33	296.0	78.4	167.6	4.50 ± 2.50	$0.097_{-0.076}^{+0.117}$	$38.648_{-1.696}^{+0.917}$	1
20180916C	107.15	45.08	2248.3	69.3	2129.0	2.10 ± 1.10	$2.682_{-0.578}^{+0.378}$	$41.433_{-0.540}^{+0.299}$	0
20180917B	238.80	77.53	860.5	46.6	763.9	8.30 ± 3.20	$0.875_{-0.314}^{+0.191}$	$40.986_{-0.641}^{+0.331}$	1
20180918A	301.27	64.96	1454.1	80.1	1324.0	4.10 ± 1.30	$1.576_{-0.383}^{+0.278}$	$41.239_{-0.429}^{+0.270}$	1
20180919B	5.34	5.94	558.0	30.6	477.4	3.00 ± 1.20	$0.512_{-0.287}^{+0.154}$	$40.026_{-1.004}^{+0.400}$	1
20180920A	78.89	28.29	562.9	168.0	344.9	8.50 ± 4.80	$0.337_{-0.245}^{+0.142}$	$40.075_{-1.571}^{+0.532}$	1

— Continued from previous page

FRBs	RA [°]	Dec [°]	DM _{obs} [pc/cm ³]	DM _{MW} [pc/cm ³]	DM _E [pc/cm ³]	Fluence [Jy ms]	z_{inf}	$\log(E/\text{erg})$	flag
20180920B	191.09	63.52	459.4	29.2	380.2	1.70±0.53	0.391 ^{+0.138} _{-0.276}	39.520 ^{+0.409} _{-1.306}	0
20180921A	28.92	5.05	393.1	33.9	309.2	2.30±1.60	0.285 ^{+0.144} _{-0.208}	39.350 ^{+0.621} _{-1.719}	0
20180922A	342.29	69.67	562.9	148.5	364.4	7.70±5.50	0.367 ^{+0.139} _{-0.268}	40.114 ^{+0.543} _{-1.762}	1
20180923A	327.61	71.92	218.4	99.0	69.4	1.20±0.70	—	—	1
20180923C	239.14	22.85	173.1	28.2	94.9	1.37±0.55	—	—	1
20180923D	169.08	48.75	328.4	29.7	248.7	2.20±1.30	0.209 ^{+0.128} _{-0.156}	39.039 ^{+0.652} _{-1.629}	1
20180924A	35.46	37.52	1114.5	67.2	997.3	3.50±1.20	1.180 ^{+0.206} _{-0.357}	40.898 ^{+0.280} _{-0.528}	1
20180925A	74.93	77.99	236.2	69.1	117.1	8.70±4.40	0.041 ^{+0.093} _{-0.039}	38.160 ^{+1.240} _{-3.158}	0
20180925B	145.45	20.99	668.0	39.8	578.2	2.70±1.10	0.649 ^{+0.160} _{-0.332}	40.210 ^{+0.362} _{-0.917}	1
20180928A	312.95	30.85	250.7	156.0	44.7	2.50±0.97	—	—	0
20181012B	206.33	64.15	713.3	31.6	631.7	1.44±0.51	0.712 ^{+0.167} _{-0.298}	40.027 ^{+0.335} _{-0.713}	0
20181013A	262.83	38.41	308.9	47.7	211.2	3.50±1.20	0.158 ^{+0.121} _{-0.119}	38.978 ^{+0.660} _{-1.448}	1
20181013B	97.18	52.04	284.7	93.0	141.7	21.00±11.00	0.069 ^{+0.105} _{-0.057}	38.999 ^{+1.029} _{-1.914}	0
20181013C	146.07	34.10	1004.5	37.3	917.2	1.64±0.88	1.079 ^{+0.198} _{-0.345}	40.483 ^{+0.347} _{-0.705}	1
20181013E	307.28	69.02	344.5	80.0	214.5	2.03±0.53	0.162 ^{+0.121} _{-0.122}	38.768 ^{+0.622} _{-1.395}	0
20181014A	46.01	63.33	1311.8	183.6	1078.2	2.70±1.50	1.278 ^{+0.223} _{-0.399}	40.861 ^{+0.343} _{-0.710}	1
20181014B	78.56	14.66	888.0	102.6	735.4	1.88±0.59	0.843 ^{+0.182} _{-0.335}	40.305 ^{+0.307} _{-0.655}	1
20181014C	117.87	41.59	752.1	59.8	642.3	1.48±0.55	0.727 ^{+0.167} _{-0.303}	40.058 ^{+0.337} _{-0.723}	0
20181014D	216.04	-2.93	376.9	29.8	297.1	18.00±11.00	0.270 ^{+0.143} _{-0.198}	40.192 ^{+0.612} _{-1.618}	1
20181015A	175.76	83.58	567.7	45.4	472.3	3.40±1.90	0.505 ^{+0.155} _{-0.283}	40.066 ^{+0.452} _{-1.140}	0
20181017B	237.76	78.50	304.1	40.4	213.7	6.50±3.60	0.161 ^{+0.121} _{-0.122}	39.267 ^{+0.716} _{-1.614}	1
20181018A	17.03	51.55	1132.2	123.7	958.5	5.80±3.20	1.132 ^{+0.201} _{-0.341}	41.077 ^{+0.346} _{-0.693}	0
20181018B	336.82	71.91	292.8	112.1	130.7	7.90±5.20	0.056 ^{+0.100} _{-0.049}	38.398 ^{+1.142} _{-2.306}	1
20181018C	67.15	37.57	409.2	144.2	215.0	3.30±1.40	0.163 ^{+0.121} _{-0.123}	38.983 ^{+0.674} _{-1.503}	1
20181019B	37.87	68.18	723.0	157.6	515.4	2.70±1.10	0.569 ^{+0.149} _{-0.313}	40.083 ^{+0.374} _{-0.992}	0
20181019C	244.70	66.27	503.0	40.6	412.4	2.10±1.20	0.432 ^{+0.145} _{-0.275}	39.707 ^{+0.475} _{-1.325}	0
20181020A	322.62	78.83	1111.2	70.9	990.3	4.90±2.90	1.171 ^{+0.205} _{-0.353}	41.037 ^{+0.355} _{-0.734}	0
20181022C	141.56	83.81	528.9	50.3	428.6	3.20±2.20	0.451 ^{+0.149} _{-0.274}	39.932 ^{+0.504} _{-1.389}	1
20181022D	179.18	36.53	512.7	18.5	444.2	6.20±2.80	0.470 ^{+0.152} _{-0.273}	40.258 ^{+0.432} _{-1.084}	1
20181022E	221.18	27.13	286.3	22.1	214.2	2.08±0.84	0.162 ^{+0.121} _{-0.122}	38.776 ^{+0.670} _{-1.488}	1
20181025A	105.78	64.25	590.4	59.5	480.9	2.68±0.99	0.518 ^{+0.153} _{-0.289}	39.987 ^{+0.388} _{-0.980}	1
20181027A	131.90	-4.24	726.3	62.6	613.7	22.00±15.00	0.690 ^{+0.166} _{-0.294}	41.180 ^{+0.434} _{-1.033}	1
20181030C	309.83	3.99	668.0	72.3	545.7	5.50±3.60	0.612 ^{+0.151} _{-0.331}	40.461 ^{+0.432} _{-1.210}	0
20181030D	81.79	16.07	289.5	123.6	115.9	5.90±1.90	0.040 ^{+0.092} _{-0.039}	37.962 ^{+1.199} _{-3.303}	1
20181030E	135.67	8.89	158.5	48.7	59.8	6.30±3.90	—	—	1
20181101A	21.26	53.88	1468.7	140.9	1277.8	10.70±5.20	1.527 ^{+0.261} _{-0.384}	41.627 ^{+0.319} _{-0.563}	1
20181102A	87.22	15.63	415.7	156.9	208.8	2.52±0.92	0.154 ^{+0.121} _{-0.117}	38.815 ^{+0.675} _{-1.465}	0
20181104C	77.05	17.44	580.7	105.2	425.5	20.70±5.70	0.448 ^{+0.149} _{-0.274}	40.735 ^{+0.382} _{-1.036}	1
20181115A	142.98	56.40	981.8	40.2	891.6	1.92±0.47	1.045 ^{+0.198} _{-0.345}	40.521 ^{+0.261} _{-0.509}	1
20181116A	36.05	4.52	354.2	35.9	268.3	5.23±0.91	0.234 ^{+0.135} _{-0.173}	39.519 ^{+0.501} _{-1.308}	1
20181116B	232.66	64.94	409.2	35.7	323.5	1.92±0.40	0.304 ^{+0.146} _{-0.221}	39.331 ^{+0.457} _{-1.300}	1
20181117A	147.73	52.51	960.8	39.6	871.2	3.10±1.70	1.017 ^{+0.198} _{-0.337}	40.703 ^{+0.360} _{-0.733}	1

— Continued from previous page

FRBs	RA [°]	Dec [°]	DM _{obs} [pc/cm ³]	DM _{MW} [pc/cm ³]	DM _E [pc/cm ³]	Fluence [Jy ms]	z_{inf}	$\log(E/\text{erg})$	flag
20181117B	81.09	79.99	540.2	67.0	423.2	11.00 ± 6.90	0.445 ^{+0.148} _{-0.274}	40.454 ^{+0.489} _{-1.335}	1
20181117C	53.21	25.73	1776.0	68.4	1657.6	3.00 ± 1.10	2.026 ^{+0.305} _{-0.495}	41.336 ^{+0.263} _{-0.457}	1
20181118A	20.65	-6.41	558.0	32.1	475.9	10.00 ± 5.00	0.510 ^{+0.154} _{-0.286}	40.545 ^{+0.432} _{-1.084}	0
20181118B	58.28	10.79	422.2	53.0	319.2	3.20 ± 1.90	0.298 ^{+0.146} _{-0.217}	39.534 ^{+0.583} _{-1.590}	1
20181119B	299.38	31.12	608.2	441.4	116.8	94.00 ± 38.00	0.041 ^{+0.093} _{-0.039}	39.187 ^{+1.213} _{-3.138}	0
20181119C	190.10	82.16	283.1	42.8	190.3	3.50 ± 1.60	0.128 ^{+0.119} _{-0.098}	38.789 ^{+0.774} _{-1.554}	1
20181119E	16.36	60.53	1169.5	220.0	899.5	2.20 ± 1.10	1.055 ^{+0.198} _{-0.346}	40.589 ^{+0.340} _{-0.684}	0
20181122A	60.04	55.48	661.6	194.9	416.7	1.42 ± 0.59	0.437 ^{+0.146} _{-0.275}	39.548 ^{+0.429} _{-1.169}	1
20181122B	281.08	85.02	224.8	53.4	121.4	22.00 ± 11.00	0.046 ^{+0.095} _{-0.043}	38.661 ^{+1.186} _{-2.614}	1
20181123A	300.76	55.87	797.4	102.5	644.9	2.50 ± 1.10	0.730 ^{+0.167} _{-0.304}	40.290 ^{+0.357} _{-0.773}	1
20181124A	175.98	63.52	1108.0	33.9	1024.1	2.60 ± 1.40	1.213 ^{+0.211} _{-0.371}	40.795 ^{+0.339} _{-0.686}	0
20181124B	318.56	29.88	800.7	104.0	646.7	4.80 ± 1.60	0.732 ^{+0.167} _{-0.305}	40.576 ^{+0.323} _{-0.697}	1
20181125A	147.94	33.93	278.2	44.0	184.2	3.20 ± 2.00	0.120 ^{+0.119} _{-0.092}	38.687 ^{+0.849} _{-1.724}	1
20181126A	262.05	81.17	493.3	48.7	394.6	9.40 ± 5.10	0.411 ^{+0.140} _{-0.277}	40.309 ^{+0.471} _{-1.393}	1
20181127A	243.80	25.43	930.1	32.0	848.1	2.90 ± 1.30	0.986 ^{+0.198} _{-0.327}	40.644 ^{+0.336} _{-0.647}	1
20181128B	157.22	38.28	454.5	31.5	373.0	1.95 ± 0.85	0.380 ^{+0.138} _{-0.274}	39.552 ^{+0.456} _{-1.441}	1
20181128C	268.77	49.71	614.6	45.4	519.2	3.40 ± 1.30	0.575 ^{+0.149} _{-0.316}	40.192 ^{+0.364} _{-0.972}	0
20181128D	215.62	59.93	147.2	33.4	63.8	7.00 ± 2.90	—	—	1
20181129A	355.12	44.95	386.6	87.4	249.2	3.10 ± 1.50	0.210 ^{+0.128} _{-0.156}	39.191 ^{+0.621} _{-1.528}	1
20181129B	307.56	81.32	406.0	62.2	293.8	9.50 ± 6.30	0.266 ^{+0.143} _{-0.195}	39.899 ^{+0.630} _{-1.682}	0
20181129C	233.38	40.03	503.0	27.3	425.7	3.60 ± 1.20	0.448 ^{+0.149} _{-0.274}	39.976 ^{+0.402} _{-1.072}	1
20181130A	355.19	46.49	218.4	93.4	75.0	1.27 ± 0.69	—	—	1
20181201A	214.96	39.27	698.7	28.3	620.4	18.90 ± 6.50	0.698 ^{+0.167} _{-0.293}	41.125 ^{+0.336} _{-0.709}	0
20181201B	273.38	56.31	875.1	49.8	775.3	2.24 ± 0.90	0.888 ^{+0.194} _{-0.305}	40.431 ^{+0.337} _{-0.630}	1
20181202A	351.01	17.36	669.6	40.4	579.2	13.70 ± 4.50	0.650 ^{+0.160} _{-0.331}	40.917 ^{+0.337} _{-0.857}	1
20181202B	202.83	64.72	826.5	34.3	742.2	4.10 ± 1.30	0.850 ^{+0.184} _{-0.330}	40.652 ^{+0.308} _{-0.641}	1
20181202C	307.13	57.03	558.0	127.3	380.7	3.40 ± 2.10	0.392 ^{+0.138} _{-0.276}	39.822 ^{+0.499} _{-1.558}	0
20181203A	33.60	23.57	635.7	46.5	539.2	3.60 ± 1.20	0.604 ^{+0.149} _{-0.329}	40.265 ^{+0.339} _{-0.930}	1
20181203B	47.31	24.02	373.6	54.9	268.7	4.50 ± 1.50	0.234 ^{+0.135} _{-0.173}	39.456 ^{+0.556} _{-1.401}	1
20181203C	198.48	72.94	2442.4	35.3	2357.1	4.80 ± 2.80	3.003 ^{+0.443} _{-0.657}	41.893 ^{+0.320} _{-0.600}	0
20181208A	264.43	62.62	561.3	43.7	467.6	4.00 ± 1.50	0.498 ^{+0.155} _{-0.281}	40.124 ^{+0.400} _{-0.992}	0
20181209A	98.16	68.69	328.4	65.4	213.0	3.20 ± 1.30	0.160 ^{+0.121} _{-0.121}	38.954 ^{+0.674} _{-1.491}	0
20181213A	127.66	73.87	677.7	47.6	580.1	3.20 ± 1.10	0.651 ^{+0.160} _{-0.330}	40.287 ^{+0.341} _{-0.863}	1
20181213B	183.52	53.70	626.0	30.0	546.0	1.70 ± 1.00	0.612 ^{+0.151} _{-0.331}	39.952 ^{+0.415} _{-1.133}	1
20181213C	216.40	47.46	380.1	29.9	300.2	1.86 ± 0.99	0.274 ^{+0.143} _{-0.200}	39.219 ^{+0.587} _{-1.537}	0
20181214A	70.00	43.07	467.5	183.6	233.9	0.41 ± 0.17	0.189 ^{+0.124} _{-0.142}	38.217 ^{+0.623} _{-1.484}	1
20181214B	138.79	42.15	1120.9	42.2	1028.7	1.23 ± 0.41	1.218 ^{+0.212} _{-0.373}	40.474 ^{+0.276} _{-0.527}	0
20181214C	175.93	60.02	632.4	32.9	549.5	5.00 ± 1.60	0.616 ^{+0.152} _{-0.332}	40.426 ^{+0.334} _{-0.912}	1
20181214D	178.57	46.71	1171.1	19.8	1101.3	9.00 ± 4.30	1.307 ^{+0.224} _{-0.411}	41.405 ^{+0.318} _{-0.643}	0
20181214F	252.62	32.44	2106.0	40.5	2015.5	2.21 ± 0.86	2.527 ^{+0.362} _{-0.562}	41.403 ^{+0.262} _{-0.442}	0
20181215A	93.38	39.34	412.5	128.4	234.1	0.72 ± 0.20	0.190 ^{+0.124} _{-0.142}	38.463 ^{+0.579} _{-1.393}	0
20181215B	254.81	47.56	493.3	39.9	403.4	2.90 ± 1.50	0.421 ^{+0.142} _{-0.276}	39.822 ^{+0.462} _{-1.320}	1

— Continued from previous page

FRBs	RA [°]	Dec [°]	DM _{obs} [pc/cm ³]	DM _{MW} [pc/cm ³]	DM _E [pc/cm ³]	Fluence [Jy ms]	z_{inf}	$\log(E/\text{erg})$	flag
20181216A	306.28	53.53	541.9	145.9	346.0	1.70 ± 1.10	0.338 ^{+0.142} _{-0.247}	39.381 ^{+0.552} _{-1.662}	0
20181217A	290.50	59.80	1175.9	68.5	1057.4	1.76 ± 0.63	1.253 ^{+0.218} _{-0.388}	40.656 ^{+0.284} _{-0.548}	1
20181218A	5.06	71.35	1873.1	145.9	1677.2	1.59 ± 0.98	2.051 ^{+0.312} _{-0.503}	41.071 ^{+0.337} _{-0.676}	1
20181218B	18.04	69.39	752.1	168.3	533.8	1.80 ± 1.50	0.597 ^{+0.148} _{-0.326}	39.952 ^{+0.478} _{-1.536}	0
20181218C	285.98	58.24	385.0	65.2	269.8	1.73 ± 0.73	0.236 ^{+0.135} _{-0.174}	39.046 ^{+0.583} _{-1.462}	0
20181219B	180.79	71.55	1950.7	35.8	1864.9	27.00 ± 22.00	2.300 ^{+0.357} _{-0.511}	42.405 ^{+0.388} _{-0.962}	1
20181219C	17.77	14.11	648.6	36.9	561.7	0.57 ± 0.19	0.630 ^{+0.156} _{-0.337}	39.505 ^{+0.339} _{-0.910}	1
20181220A	346.11	48.43	208.7	125.1	33.6	3.00 ± 1.70	—	—	1
20181220B	277.37	84.87	257.2	53.0	154.2	3.80 ± 2.60	0.082 ^{+0.111} _{-0.066}	38.424 ^{+1.008} _{-1.942}	1
20181221A	230.58	25.86	313.8	22.0	241.8	5.80 ± 2.00	0.201 ^{+0.125} _{-0.150}	39.421 ^{+0.586} _{-1.432}	1
20181221B	306.31	80.98	1392.7	59.6	1283.1	3.30 ± 1.70	1.533 ^{+0.263} _{-0.384}	41.119 ^{+0.328} _{-0.587}	1
20181222B	90.04	38.55	619.5	148.5	421.0	0.83 ± 0.51	0.442 ^{+0.147} _{-0.275}	39.326 ^{+0.486} _{-1.330}	0
20181222C	131.05	68.33	1104.8	46.3	1008.5	2.90 ± 1.30	1.194 ^{+0.207} _{-0.363}	40.827 ^{+0.313} _{-0.606}	0
20181222D	188.20	56.16	1413.7	27.8	1335.9	1.23 ± 0.82	1.588 ^{+0.283} _{-0.384}	40.724 ^{+0.374} _{-0.738}	0
20181222E	50.64	86.97	328.4	60.3	218.1	5.50 ± 3.20	0.167 ^{+0.121} _{-0.126}	39.229 ^{+0.710} _{-1.639}	1
20181223B	174.89	21.59	564.5	24.3	490.2	4.10 ± 1.10	0.532 ^{+0.152} _{-0.296}	40.197 ^{+0.347} _{-0.911}	1
20181223C	181.05	27.58	111.6	19.0	42.6	2.84 ± 0.93	—	—	1
20181224A	355.11	44.56	308.9	83.7	175.2	3.30 ± 1.80	0.107 ^{+0.118} _{-0.083}	38.599 ^{+0.875} _{-1.658}	1
20181224B	45.36	46.14	779.6	119.9	609.7	3.10 ± 1.70	0.686 ^{+0.165} _{-0.298}	40.322 ^{+0.399} _{-0.897}	1
20181224C	115.29	60.28	608.2	67.2	491.0	9.60 ± 3.20	0.533 ^{+0.152} _{-0.296}	40.569 ^{+0.368} _{-0.951}	0
20181224D	182.45	54.85	690.7	31.9	608.8	1.95 ± 0.98	0.684 ^{+0.165} _{-0.299}	40.119 ^{+0.386} _{-0.858}	0
20181224E	239.32	7.32	580.7	35.4	495.3	10.30 ± 4.90	0.539 ^{+0.151} _{-0.299}	40.611 ^{+0.408} _{-1.054}	1
20181225B	36.77	88.20	299.2	58.2	191.0	7.50 ± 3.80	0.129 ^{+0.120} _{-0.099}	39.127 ^{+0.785} _{-1.594}	1
20181226B	182.66	12.43	287.9	28.6	209.3	52.00 ± 17.00	0.155 ^{+0.121} _{-0.117}	40.134 ^{+0.661} _{-1.439}	1
20181226C	349.05	44.94	409.2	94.2	265.0	2.70 ± 1.40	0.230 ^{+0.134} _{-0.170}	39.215 ^{+0.616} _{-1.545}	1
20181226D	120.22	22.16	386.6	66.2	270.4	3.00 ± 1.40	0.237 ^{+0.136} _{-0.175}	39.289 ^{+0.596} _{-1.497}	1
20181226E	303.56	73.64	308.9	69.0	189.9	1.35 ± 0.77	0.128 ^{+0.119} _{-0.098}	38.371 ^{+0.808} _{-1.656}	1
20181227A	31.79	78.38	791.0	88.8	652.2	1.82 ± 0.91	0.740 ^{+0.167} _{-0.308}	40.165 ^{+0.373} _{-0.821}	0
20181228A	7.26	10.22	748.9	34.4	664.5	4.00 ± 2.10	0.756 ^{+0.168} _{-0.313}	40.528 ^{+0.377} _{-0.841}	1
20181228B	250.43	63.85	566.1	37.4	478.7	1.67 ± 0.77	0.514 ^{+0.154} _{-0.288}	39.775 ^{+0.418} _{-1.050}	1
20181228C	265.19	54.36	509.5	44.4	415.1	0.74 ± 0.25	0.435 ^{+0.146} _{-0.275}	39.261 ^{+0.405} _{-1.123}	0
20181229A	137.18	42.01	955.9	43.3	862.6	4.00 ± 1.30	1.006 ^{+0.198} _{-0.333}	40.803 ^{+0.294} _{-0.559}	1
20181229B	238.37	19.78	375.3	15.6	309.7	4.90 ± 3.40	0.286 ^{+0.145} _{-0.208}	39.680 ^{+0.620} _{-1.716}	0
20181230A	346.69	83.37	763.5	62.3	651.2	18.00 ± 10.00	0.738 ^{+0.167} _{-0.307}	41.158 ^{+0.389} _{-0.872}	0
20181230B	20.83	79.70	1135.5	83.1	1002.4	9.70 ± 4.80	1.186 ^{+0.207} _{-0.360}	41.345 ^{+0.327} _{-0.643}	1
20181230C	245.75	50.52	1036.8	36.5	950.3	2.10 ± 1.20	1.121 ^{+0.200} _{-0.342}	40.627 ^{+0.352} _{-0.718}	1
20181230D	255.30	50.51	224.8	41.4	133.4	2.00 ± 1.20	0.059 ^{+0.101} _{-0.051}	37.848 ^{+1.106} _{-2.159}	1
20181230E	113.26	86.85	1041.7	54.5	937.2	10.40 ± 5.70	1.105 ^{+0.198} _{-0.344}	41.308 ^{+0.347} _{-0.703}	1
20181231A	29.71	20.96	1376.5	42.8	1283.7	2.20 ± 1.10	1.534 ^{+0.263} _{-0.384}	40.944 ^{+0.323} _{-0.573}	1
20181231B	128.77	55.99	199.0	48.7	100.3	2.34 ± 0.73	0.022 ^{+0.084} _{-0.021}	37.052 ^{+1.510} _{-2.867}	1
20181231C	197.09	69.18	554.8	34.2	470.6	1.20 ± 0.54	0.502 ^{+0.155} _{-0.282}	39.609 ^{+0.422} _{-1.045}	1
20190101A	171.01	27.99	867.0	36.7	780.3	11.30 ± 3.40	0.893 ^{+0.195} _{-0.301}	41.140 ^{+0.304} _{-0.553}	0

— Continued from previous page

FRBs	RA [°]	Dec [°]	DM _{obs} [pc/cm ³]	DM _{MW} [pc/cm ³]	DM _E [pc/cm ³]	Fluence [Jy ms]	z_{inf}	$\log(E/\text{erg})$	flag
20190101B	307.77	29.89	1321.5	231.6	1039.9	4.40 ± 2.50	1.232 ^{+0.214} _{-0.379}	41.038 ^{+0.347} _{-0.717}	1
20190102A	9.26	26.72	697.1	41.5	605.6	4.20 ± 1.70	0.681 ^{+0.165} _{-0.303}	40.447 ^{+0.357} _{-0.793}	1
20190102B	21.66	21.39	367.2	41.1	276.1	3.90 ± 1.70	0.244 ^{+0.138} _{-0.179}	39.430 ^{+0.583} _{-1.468}	1
20190103B	93.57	19.73	530.5	176.5	304.0	12.90 ± 6.90	0.279 ^{+0.144} _{-0.203}	40.077 ^{+0.583} _{-1.537}	1
20190103C	104.19	11.07	1349.0	155.4	1143.6	13.40 ± 7.10	1.360 ^{+0.224} _{-0.385}	41.616 ^{+0.328} _{-0.645}	1
20190103D	221.84	59.91	1911.9	31.6	1830.3	1.17 ± 0.44	2.257 ^{+0.346} _{-0.507}	41.025 ^{+0.267} _{-0.438}	0
20190103E	262.89	45.84	736.0	45.4	640.6	2.00 ± 1.10	0.724 ^{+0.167} _{-0.302}	40.185 ^{+0.391} _{-0.869}	0
20190104A	70.50	35.59	548.3	150.4	347.9	3.90 ± 1.90	0.341 ^{+0.141} _{-0.249}	39.750 ^{+0.505} _{-1.501}	1
20190104B	234.72	-6.25	527.3	47.0	430.3	9.50 ± 5.60	0.453 ^{+0.150} _{-0.274}	40.409 ^{+0.477} _{-1.263}	0
20190105A	266.30	63.82	385.0	47.8	287.2	3.50 ± 1.50	0.258 ^{+0.142} _{-0.189}	39.436 ^{+0.572} _{-1.456}	0
20190106A	22.19	46.12	341.3	90.1	201.2	0.81 ± 0.45	0.144 ^{+0.120} _{-0.109}	38.257 ^{+0.758} _{-1.627}	0
20190106B	335.63	46.13	315.4	140.5	124.9	3.80 ± 2.40	0.050 ^{+0.097} _{-0.045}	37.972 ^{+1.187} _{-2.513}	1
20190107A	0.86	21.81	841.1	31.8	759.3	6.30 ± 3.90	0.870 ^{+0.189} _{-0.317}	40.860 ^{+0.399} _{-0.858}	0
20190107B	33.45	83.40	166.6	70.5	46.1	4.30 ± 2.50	—	—	1
20190109A	107.96	5.16	325.1	148.2	126.9	6.40 ± 2.60	0.052 ^{+0.098} _{-0.047}	38.237 ^{+1.103} _{-2.208}	0
20190109B	253.47	1.25	176.3	69.4	56.9	3.00 ± 1.70	—	—	0
20190110A	64.95	47.44	470.7	186.5	234.2	3.80 ± 2.30	0.190 ^{+0.124} _{-0.142}	39.186 ^{+0.677} _{-1.655}	1
20190110B	131.68	50.16	486.9	46.3	390.6	1.90 ± 1.40	0.406 ^{+0.139} _{-0.277}	39.603 ^{+0.523} _{-1.658}	1
20190110C	246.98	41.42	221.6	35.3	136.3	1.40 ± 0.76	0.062 ^{+0.102} _{-0.053}	37.741 ^{+1.069} _{-2.032}	1
20190111A	217.00	26.78	173.1	22.6	100.5	17.00 ± 7.20	0.022 ^{+0.084} _{-0.021}	37.922 ^{+1.540} _{-2.953}	1
20190111B	260.02	13.53	1334.4	62.6	1221.8	0.78 ± 0.28	1.461 ^{+0.247} _{-0.379}	40.448 ^{+0.279} _{-0.478}	1
20190112A	257.98	61.20	420.5	36.7	333.8	16.20 ± 6.40	0.320 ^{+0.144} _{-0.233}	40.306 ^{+0.501} _{-1.422}	0
20190113A	108.14	-2.99	430.3	180.3	200.0	5.60 ± 3.40	0.142 ^{+0.120} _{-0.108}	39.086 ^{+0.777} _{-1.682}	0
20190114A	8.95	19.17	889.6	40.3	799.3	2.30 ± 1.40	0.918 ^{+0.198} _{-0.304}	40.475 ^{+0.394} _{-0.796}	0
20190115A	45.61	54.28	1020.6	185.3	785.3	0.95 ± 0.56	0.899 ^{+0.197} _{-0.298}	40.071 ^{+0.392} _{-0.776}	0
20190115B	76.82	82.06	748.9	64.4	634.5	5.20 ± 3.10	0.716 ^{+0.167} _{-0.299}	40.589 ^{+0.406} _{-0.917}	1
20190116C	249.32	70.96	629.2	41.8	537.4	65.00 ± 26.00	0.602 ^{+0.149} _{-0.328}	41.518 ^{+0.360} _{-0.977}	1
20190116D	85.10	68.68	1161.4	75.9	1035.5	4.70 ± 1.70	1.227 ^{+0.213} _{-0.377}	41.063 ^{+0.286} _{-0.547}	0
20190116E	19.36	52.32	1489.7	127.1	1312.6	1.12 ± 0.75	1.564 ^{+0.274} _{-0.384}	40.669 ^{+0.372} _{-0.747}	0
20190116F	261.67	75.00	315.4	45.3	220.1	1.54 ± 0.62	0.170 ^{+0.122} _{-0.128}	38.692 ^{+0.652} _{-1.483}	1
20190117C	115.13	74.59	865.4	52.8	762.6	0.79 ± 0.22	0.873 ^{+0.190} _{-0.315}	39.963 ^{+0.296} _{-0.574}	0
20190117D	208.87	31.68	1175.9	20.4	1105.5	3.50 ± 1.50	1.312 ^{+0.224} _{-0.413}	40.998 ^{+0.303} _{-0.605}	1
20190118A	253.31	11.55	224.8	53.1	121.7	18.00 ± 6.60	0.046 ^{+0.095} _{-0.043}	38.581 ^{+1.143} _{-2.487}	1
20190118B	39.71	23.57	666.4	45.7	570.7	3.62 ± 0.99	0.641 ^{+0.159} _{-0.340}	40.324 ^{+0.319} _{-0.866}	0
20190121A	354.74	78.60	423.8	85.8	288.0	10.80 ± 6.30	0.259 ^{+0.142} _{-0.190}	39.929 ^{+0.616} _{-1.593}	1
20190122A	349.56	37.50	1229.3	62.7	1116.6	5.70 ± 2.80	1.326 ^{+0.224} _{-0.408}	41.220 ^{+0.320} _{-0.645}	0
20190122B	2.53	35.12	467.5	52.4	365.1	1.75 ± 0.76	0.368 ^{+0.139} _{-0.269}	39.473 ^{+0.465} _{-1.466}	0
20190122C	200.60	17.57	690.7	25.2	615.5	47.00 ± 30.00	0.692 ^{+0.166} _{-0.292}	41.512 ^{+0.422} _{-0.971}	1
20190124A	50.46	51.58	1274.6	175.3	1049.3	13.40 ± 9.30	1.243 ^{+0.216} _{-0.384}	41.531 ^{+0.380} _{-0.868}	0
20190124B	214.69	28.80	443.2	23.4	369.8	11.70 ± 4.40	0.375 ^{+0.139} _{-0.273}	40.317 ^{+0.441} _{-1.421}	1
20190124C	217.17	28.38	302.5	20.3	232.2	13.70 ± 7.70	0.187 ^{+0.123} _{-0.140}	39.729 ^{+0.670} _{-1.611}	1
20190124D	237.26	81.23	341.3	46.8	244.5	1.90 ± 1.10	0.204 ^{+0.126} _{-0.152}	38.952 ^{+0.653} _{-1.621}	0

— Continued from previous page

FRBs	RA [°]	Dec [°]	DM _{obs} [pc/cm ³]	DM _{MW} [pc/cm ³]	DM _E [pc/cm ³]	Fluence [Jy ms]	z_{inf}	$\log(E/\text{erg})$	flag
20190124E	297.75	20.57	614.6	388.8	175.8	7.30±4.90	0.108 ^{+0.118} _{-0.083}	38.951 ^{+0.906} _{-1.798}	1
20190124F	338.92	5.30	253.9	36.7	167.2	6.40±3.20	0.097 ^{+0.117} _{-0.076}	38.796 ^{+0.903} _{-1.647}	1
20190125A	45.73	27.81	562.9	58.6	454.3	2.60±1.20	0.482 ^{+0.153} _{-0.275}	39.906 ^{+0.431} _{-1.073}	0
20190125B	231.45	50.54	177.9	32.9	95.0	4.70±2.70	—	—	0
20190127B	150.92	83.56	666.4	51.8	564.6	11.40±5.80	0.633 ^{+0.157} _{-0.338}	40.811 ^{+0.393} _{-1.040}	0
20190128A	21.80	24.67	695.5	43.0	602.5	2.00±1.00	0.677 ^{+0.164} _{-0.306}	40.120 ^{+0.386} _{-0.881}	0
20190128B	127.44	23.29	247.5	56.5	141.0	1.64±0.47	0.068 ^{+0.105} _{-0.057}	37.882 ^{+0.960} _{-1.750}	1
20190128C	69.80	78.94	304.1	64.8	189.3	5.90±4.20	0.127 ^{+0.119} _{-0.097}	39.006 ^{+0.848} _{-1.830}	0
20190128D	283.32	17.44	428.6	231.2	147.4	3.60±2.80	0.075 ^{+0.108} _{-0.061}	38.313 ^{+1.064} _{-2.166}	0
20190129A	45.06	21.42	478.8	46.1	382.7	5.00±3.10	0.395 ^{+0.138} _{-0.277}	39.997 ^{+0.498} _{-1.548}	0
20190130A	25.64	13.16	1365.2	35.1	1280.1	4.40±1.80	1.530 ^{+0.262} _{-0.384}	41.242 ^{+0.296} _{-0.502}	0
20190130B	172.11	16.05	988.3	29.0	909.3	2.95±0.94	1.068 ^{+0.198} _{-0.345}	40.729 ^{+0.282} _{-0.543}	1
20190131B	354.72	11.71	1801.9	31.8	1720.1	3.30±1.30	2.106 ^{+0.325} _{-0.523}	41.412 ^{+0.274} _{-0.480}	1
20190131C	166.45	10.43	506.3	31.5	424.8	2.10±1.60	0.447 ^{+0.148} _{-0.274}	39.739 ^{+0.523} _{-1.523}	1
20190131D	57.46	22.75	642.1	67.5	524.6	6.80±3.70	0.583 ^{+0.149} _{-0.320}	40.507 ^{+0.409} _{-1.102}	1
20190131E	195.65	80.92	279.8	43.3	186.5	5.10±3.40	0.123 ^{+0.119} _{-0.094}	38.914 ^{+0.849} _{-1.771}	1
20190201A	64.03	84.84	241.0	61.4	129.6	3.10±1.60	0.055 ^{+0.099} _{-0.048}	37.972 ^{+1.112} _{-2.191}	0
20190201B	118.20	55.58	748.9	53.9	645.0	2.30±1.20	0.730 ^{+0.167} _{-0.304}	40.254 ^{+0.381} _{-0.841}	1
20190202A	344.20	17.10	305.7	39.1	216.6	95.00±41.00	0.165 ^{+0.121} _{-0.124}	40.455 ^{+0.671} _{-1.507}	1
20190202B	114.32	32.45	464.2	69.4	344.8	2.70±1.30	0.337 ^{+0.142} _{-0.245}	39.577 ^{+0.508} _{-1.495}	0
20190203A	133.68	70.82	418.9	44.2	324.7	4.00±1.90	0.306 ^{+0.145} _{-0.222}	39.655 ^{+0.541} _{-1.479}	1
20190203B	130.64	61.89	580.7	44.3	486.4	0.93±0.48	0.526 ^{+0.152} _{-0.293}	39.543 ^{+0.427} _{-1.093}	0
20190203C	196.01	2.48	370.4	29.6	290.8	4.40±3.00	0.262 ^{+0.142} _{-0.192}	39.552 ^{+0.639} _{-1.709}	0
20190204A	161.33	61.53	448.0	34.5	363.5	1.50±0.70	0.365 ^{+0.139} _{-0.267}	39.400 ^{+0.476} _{-1.491}	0
20190204B	255.92	75.87	1463.8	44.4	1369.4	4.40±1.80	1.638 ^{+0.280} _{-0.406}	41.306 ^{+0.295} _{-0.497}	1
20190205A	342.22	83.37	693.9	66.2	577.7	1.70±0.74	0.649 ^{+0.160} _{-0.333}	40.008 ^{+0.370} _{-0.940}	0
20190206A	244.85	9.36	187.6	40.7	96.9	9.10±7.00	—	—	1
20190206B	49.76	79.50	355.8	81.8	224.0	9.60±6.30	0.176 ^{+0.122} _{-0.132}	39.516 ^{+0.714} _{-1.721}	0
20190206C	200.45	74.39	1044.9	40.2	954.7	3.80±2.00	1.127 ^{+0.200} _{-0.341}	40.890 ^{+0.339} _{-0.672}	0
20190208B	91.00	80.88	713.3	59.7	603.6	14.30±6.30	0.678 ^{+0.164} _{-0.305}	40.976 ^{+0.368} _{-0.828}	1
20190208C	141.55	83.56	237.8	49.1	138.7	1.74±0.88	0.065 ^{+0.104} _{-0.055}	37.873 ^{+1.042} _{-1.950}	1
20190210B	104.18	23.70	622.7	115.0	457.7	5.30±1.50	0.486 ^{+0.153} _{-0.277}	40.223 ^{+0.374} _{-0.944}	1
20190210C	295.75	89.10	642.1	54.0	538.1	3.60±1.20	0.603 ^{+0.149} _{-0.328}	40.263 ^{+0.339} _{-0.931}	1
20190210D	307.80	55.46	357.5	139.6	167.9	2.50±0.47	0.098 ^{+0.117} _{-0.076}	38.395 ^{+0.798} _{-1.433}	0
20190210E	313.65	86.67	580.7	58.0	472.7	1.45±0.29	0.505 ^{+0.155} _{-0.283}	39.697 ^{+0.338} _{-0.881}	0
20190211A	67.06	68.64	1188.9	104.5	1034.4	5.80±1.60	1.225 ^{+0.213} _{-0.376}	41.153 ^{+0.257} _{-0.492}	1
20190211B	299.62	61.37	260.4	84.2	126.2	1.35±0.38	0.051 ^{+0.097} _{-0.046}	37.548 ^{+1.069} _{-2.157}	1
20190212B	139.99	52.11	600.1	41.1	509.0	3.70±1.70	0.560 ^{+0.149} _{-0.309}	40.203 ^{+0.393} _{-1.034}	1
20190212C	172.57	28.14	1012.6	18.5	944.1	12.20±3.50	1.114 ^{+0.199} _{-0.343}	41.385 ^{+0.266} _{-0.501}	0
20190212D	178.83	66.72	1145.2	40.8	1054.4	5.70±3.70	1.249 ^{+0.217} _{-0.387}	41.164 ^{+0.369} _{-0.810}	0
20190213C	64.26	45.00	357.5	176.4	131.1	1.09±0.59	0.057 ^{+0.100} _{-0.050}	37.545 ^{+1.107} _{-2.165}	0
20190213D	336.45	52.71	1344.1	231.8	1062.3	2.20±1.20	1.259 ^{+0.219} _{-0.391}	40.758 ^{+0.341} _{-0.698}	1

— Continued from previous page

FRBs	RA [°]	Dec [°]	DM _{obs} [pc/cm ³]	DM _{MW} [pc/cm ³]	DM _E [pc/cm ³]	Fluence [Jy ms]	z_{inf}	$\log(E/\text{erg})$	flag
20190214A	96.09	66.24	498.2	70.3	377.9	8.80 ± 2.30	0.388 ^{+0.138} _{-0.276}	40.225 ^{+0.394} _{-1.291}	0
20190214C	218.87	19.36	533.8	22.8	461.0	5.20 ± 2.20	0.490 ^{+0.154} _{-0.278}	40.223 ^{+0.417} _{-1.035}	1
20190215B	335.04	45.34	273.4	135.0	88.4	5.60 ± 2.50	—	—	1
20190217A	94.88	43.11	797.4	110.0	637.4	1.19 ± 0.39	0.720 ^{+0.167} _{-0.301}	39.954 ^{+0.325} _{-0.695}	1
20190217B	22.58	26.95	847.6	47.2	750.4	6.00 ± 2.20	0.860 ^{+0.187} _{-0.324}	40.828 ^{+0.325} _{-0.656}	0
20190218A	184.05	56.42	1282.7	29.0	1203.7	1.65 ± 0.71	1.438 ^{+0.242} _{-0.378}	40.758 ^{+0.301} _{-0.534}	1
20190218B	268.70	17.93	549.9	83.6	416.3	5.90 ± 1.60	0.437 ^{+0.146} _{-0.275}	40.166 ^{+0.383} _{-1.075}	0
20190218C	156.96	77.95	318.6	43.0	225.6	31.00 ± 18.00	0.178 ^{+0.122} _{-0.134}	40.037 ^{+0.689} _{-1.633}	1
20190219A	105.78	43.13	655.1	76.7	528.4	0.96 ± 0.22	0.589 ^{+0.149} _{-0.322}	39.666 ^{+0.307} _{-0.872}	1
20190219B	246.30	57.92	1675.7	32.3	1593.4	14.40 ± 3.40	1.947 ^{+0.294} _{-0.469}	41.980 ^{+0.220} _{-0.373}	0
20190219C	349.67	49.21	805.5	122.9	632.6	1.96 ± 0.86	0.714 ^{+0.167} _{-0.298}	40.162 ^{+0.361} _{-0.774}	0
20190220A	237.21	74.16	215.1	39.9	125.2	0.68 ± 0.44	0.050 ^{+0.097} _{-0.045}	37.230 ^{+1.188} _{-2.515}	0
20190221A	132.60	9.90	224.8	53.9	120.9	2.33 ± 0.30	0.045 ^{+0.095} _{-0.042}	37.676 ^{+1.069} _{-2.416}	1
20190221B	286.77	27.86	394.7	167.1	177.6	5.60 ± 1.40	0.111 ^{+0.119} _{-0.085}	38.857 ^{+0.769} _{-1.436}	1
20190221C	316.15	54.67	2038.0	216.3	1771.7	7.10 ± 1.60	2.182 ^{+0.330} _{-0.515}	41.777 ^{+0.215} _{-0.358}	0
20190221D	24.81	60.93	473.9	189.7	234.2	1.13 ± 0.20	0.190 ^{+0.124} _{-0.142}	38.659 ^{+0.543} _{-1.336}	0
20190222B	160.69	19.62	498.2	33.8	414.4	4.40 ± 1.80	0.434 ^{+0.145} _{-0.275}	40.033 ^{+0.428} _{-1.176}	0
20190222C	239.18	40.03	522.5	28.0	444.5	0.83 ± 0.14	0.470 ^{+0.152} _{-0.273}	39.386 ^{+0.338} _{-0.902}	1
20190222D	313.90	26.57	894.5	114.8	729.7	0.86 ± 0.28	0.836 ^{+0.180} _{-0.337}	39.958 ^{+0.311} _{-0.671}	0
20190223A	64.72	87.65	389.8	58.7	281.1	1.58 ± 0.74	0.250 ^{+0.140} _{-0.184}	39.062 ^{+0.588} _{-1.491}	1
20190223B	311.62	60.56	535.4	123.6	361.8	0.84 ± 0.20	0.363 ^{+0.139} _{-0.265}	39.141 ^{+0.405} _{-1.335}	0
20190224A	60.53	83.39	821.7	68.8	702.9	8.50 ± 3.10	0.806 ^{+0.173} _{-0.330}	40.917 ^{+0.322} _{-0.707}	0
20190224B	268.24	82.57	839.5	51.5	738.0	4.50 ± 2.60	0.846 ^{+0.183} _{-0.334}	40.687 ^{+0.387} _{-0.860}	0
20190224C	124.05	19.78	495.0	57.5	387.5	7.90 ± 3.80	0.402 ^{+0.138} _{-0.278}	40.213 ^{+0.455} _{-1.383}	1
20190224D	331.89	89.05	752.1	55.4	646.7	6.10 ± 2.00	0.732 ^{+0.167} _{-0.305}	40.680 ^{+0.322} _{-0.693}	1
20190224E	183.04	61.54	435.1	32.3	352.8	4.00 ± 0.81	0.349 ^{+0.141} _{-0.254}	39.782 ^{+0.405} _{-1.311}	1
20190226A	58.83	31.93	600.1	89.8	460.3	1.42 ± 0.43	0.489 ^{+0.154} _{-0.278}	39.657 ^{+0.379} _{-0.953}	0
20190226B	273.57	61.81	630.8	49.9	530.9	2.38 ± 0.70	0.593 ^{+0.148} _{-0.324}	40.067 ^{+0.328} _{-0.910}	0
20190226C	17.46	26.76	826.5	43.2	733.3	1.41 ± 0.35	0.840 ^{+0.182} _{-0.337}	40.177 ^{+0.285} _{-0.620}	0
20190227A	108.41	56.34	393.1	62.5	280.6	12.50 ± 2.10	0.249 ^{+0.139} _{-0.183}	39.958 ^{+0.489} _{-1.297}	1
20190227B	220.54	39.80	331.6	24.3	257.3	0.71 ± 0.15	0.220 ^{+0.131} _{-0.163}	38.595 ^{+0.525} _{-1.337}	0
20190228A	183.48	22.90	439.9	41.0	348.9	35.80 ± 4.60	0.343 ^{+0.141} _{-0.250}	40.717 ^{+0.384} _{-1.271}	0
20190228B	50.01	81.94	1125.8	81.9	993.9	66.00 ± 32.00	1.175 ^{+0.205} _{-0.355}	42.170 ^{+0.324} _{-0.633}	0
20190301B	69.50	74.08	619.5	81.0	488.5	0.85 ± 0.36	0.529 ^{+0.152} _{-0.294}	39.509 ^{+0.398} _{-1.016}	0
20190301C	171.83	34.93	805.5	23.1	732.4	2.32 ± 0.52	0.839 ^{+0.181} _{-0.338}	40.392 ^{+0.276} _{-0.608}	0
20190301D	278.72	74.68	1159.7	52.1	1057.6	1.50 ± 0.21	1.253 ^{+0.218} _{-0.388}	40.587 ^{+0.208} _{-0.421}	0
20190302A	34.80	61.34	1009.3	195.8	763.5	35.00 ± 13.00	0.874 ^{+0.191} _{-0.314}	41.610 ^{+0.327} _{-0.632}	0
20190303B	128.74	66.03	192.5	46.1	96.4	42.00 ± 19.00	—	—	1
20190303C	173.24	26.32	1088.6	22.0	1016.6	3.46 ± 0.46	1.204 ^{+0.209} _{-0.367}	40.912 ^{+0.206} _{-0.411}	1
20190303D	179.57	70.84	710.1	36.0	624.1	1.17 ± 0.67	0.702 ^{+0.167} _{-0.294}	39.923 ^{+0.403} _{-0.894}	0
20190304A	124.51	74.61	483.6	49.7	383.9	2.90 ± 1.10	0.397 ^{+0.138} _{-0.277}	39.765 ^{+0.427} _{-1.328}	1
20190304B	204.86	24.19	470.7	23.3	397.4	2.22 ± 0.59	0.414 ^{+0.141} _{-0.277}	39.690 ^{+0.384} _{-1.171}	1

— Continued from previous page

FRBs	RA [°]	Dec [°]	DM _{obs} [pc/cm ³]	DM _{MW} [pc/cm ³]	DM _E [pc/cm ³]	Fluence [Jy ms]	z_{inf}	$\log(E/\text{erg})$	flag
20190304C	223.01	26.72	564.5	21.6	492.9	1.32 ± 0.13	0.536 ^{+0.151} _{-0.298}	39.713 ^{+0.282} _{-0.819}	0
20190307A	254.55	9.85	352.6	55.3	247.3	—	0.208 ^{+0.127} _{-0.155}	—	0
20190307B	269.20	38.40	291.1	52.0	189.1	—	0.127 ^{+0.119} _{-0.097}	—	0
20190308B	38.59	83.62	179.5	68.0	61.5	1.39 ± 0.85	—	—	0
20190308C	188.36	44.39	498.2	20.8	427.4	4.80 ± 2.50	0.450 ^{+0.149} _{-0.274}	40.105 ^{+0.459} _{-1.208}	1
20190309A	278.96	52.41	357.5	59.2	248.3	0.72 ± 0.44	0.209 ^{+0.128} _{-0.155}	38.552 ^{+0.658} _{-1.652}	0
20190313B	101.98	74.13	1192.1	60.7	1081.4	2.74 ± 0.78	1.282 ^{+0.223} _{-0.400}	40.870 ^{+0.260} _{-0.504}	1
20190316A	5.23	20.51	516.0	39.0	427.0	2.53 ± 0.82	0.449 ^{+0.149} _{-0.274}	39.826 ^{+0.398} _{-1.060}	1
20190317A	87.44	44.66	1156.5	137.2	969.3	1.24 ± 0.44	1.145 ^{+0.202} _{-0.342}	40.418 ^{+0.286} _{-0.531}	0
20190317B	101.01	49.73	425.4	81.7	293.7	1.89 ± 0.46	0.266 ^{+0.143} _{-0.195}	39.198 ^{+0.504} _{-1.331}	0
20190317C	125.82	32.07	601.7	57.0	494.7	7.80 ± 2.80	0.538 ^{+0.151} _{-0.299}	40.489 ^{+0.373} _{-0.967}	0
20190317E	274.37	13.25	800.7	134.1	616.6	7.30 ± 1.80	0.693 ^{+0.166} _{-0.292}	40.705 ^{+0.304} _{-0.651}	1
20190317F	236.25	47.05	1125.8	41.0	1034.8	26.00 ± 14.00	1.226 ^{+0.213} _{-0.377}	41.805 ^{+0.339} _{-0.688}	1
20190318A	324.11	74.46	420.5	86.6	283.9	14.20 ± 2.80	0.253 ^{+0.141} _{-0.186}	40.029 ^{+0.498} _{-1.310}	1
20190319A	113.43	5.72	2041.3	109.0	1882.3	19.40 ± 4.20	2.325 ^{+0.359} _{-0.516}	42.271 ^{+0.214} _{-0.335}	1
20190320A	61.60	63.36	613.0	142.8	420.2	4.40 ± 1.40	0.441 ^{+0.147} _{-0.275}	40.049 ^{+0.398} _{-1.086}	1
20190320B	250.40	39.63	490.1	38.3	401.8	1.90 ± 0.34	0.419 ^{+0.142} _{-0.276}	39.634 ^{+0.353} _{-1.098}	1
20190320C	254.73	22.38	367.2	45.5	271.7	3.14 ± 0.65	0.238 ^{+0.136} _{-0.176}	39.315 ^{+0.511} _{-1.323}	0
20190320D	262.22	59.07	1151.7	54.2	1047.5	11.40 ± 1.60	1.241 ^{+0.216} _{-0.383}	41.459 ^{+0.209} _{-0.419}	0
20190320E	76.64	89.16	299.2	55.9	193.3	12.30 ± 4.50	0.133 ^{+0.120} _{-0.101}	39.365 ^{+0.733} _{-1.482}	1
20190322A	110.75	51.30	1054.6	58.1	946.5	10.10 ± 3.20	1.117 ^{+0.199} _{-0.342}	41.305 ^{+0.276} _{-0.518}	0
20190322B	132.03	73.34	577.4	47.4	480.0	2.04 ± 0.90	0.516 ^{+0.153} _{-0.289}	39.866 ^{+0.411} _{-1.033}	0
20190322C	296.36	70.70	1192.1	65.8	1076.3	13.00 ± 5.50	1.276 ^{+0.222} _{-0.398}	41.542 ^{+0.305} _{-0.597}	1
20190323A	112.37	34.46	855.7	71.0	734.7	2.71 ± 0.79	0.842 ^{+0.182} _{-0.336}	40.463 ^{+0.299} _{-0.643}	1
20190323B	193.22	77.24	787.7	38.4	699.3	10.60 ± 1.40	0.802 ^{+0.172} _{-0.330}	41.008 ^{+0.241} _{-0.573}	1
20190323C	199.50	40.07	380.1	22.6	307.5	1.38 ± 0.24	0.283 ^{+0.144} _{-0.206}	39.121 ^{+0.463} _{-1.286}	0
20190323D	56.88	46.93	760.2	158.9	551.3	2.49 ± 0.87	0.618 ^{+0.153} _{-0.333}	40.127 ^{+0.344} _{-0.930}	0
20190325A	130.41	83.07	357.5	49.2	258.3	4.60 ± 1.70	0.221 ^{+0.131} _{-0.164}	39.412 ^{+0.577} _{-1.433}	1
20190325B	183.92	30.32	1730.7	16.6	1664.1	3.81 ± 0.77	2.034 ^{+0.308} _{-0.498}	41.443 ^{+0.208} _{-0.357}	0
20190325C	53.85	60.17	799.0	189.6	559.4	3.83 ± 0.89	0.627 ^{+0.155} _{-0.336}	40.328 ^{+0.305} _{-0.851}	0
20190326A	161.90	74.22	283.1	40.5	192.6	1.51 ± 0.39	0.132 ^{+0.120} _{-0.100}	38.447 ^{+0.700} _{-1.415}	0
20190327A	281.31	34.28	347.8	90.0	207.8	5.20 ± 1.60	0.153 ^{+0.121} _{-0.116}	39.122 ^{+0.660} _{-1.428}	0
20190328A	120.35	59.10	1303.7	51.9	1201.8	2.66 ± 0.46	1.435 ^{+0.241} _{-0.378}	40.964 ^{+0.215} _{-0.373}	0
20190328B	199.47	86.85	564.5	49.6	464.9	2.14 ± 0.55	0.495 ^{+0.154} _{-0.279}	39.846 ^{+0.362} _{-0.920}	0
20190328C	73.83	81.96	470.7	62.5	358.2	14.90 ± 7.10	0.357 ^{+0.140} _{-0.261}	40.375 ^{+0.486} _{-1.497}	1
20190329A	65.54	73.63	189.2	88.4	50.8	2.24 ± 0.77	—	—	0
20190329B	87.90	76.27	406.0	65.9	290.1	—	0.261 ^{+0.142} _{-0.191}	—	0
20190329C	279.79	51.63	1256.8	60.8	1146.0	—	1.364 ^{+0.224} _{-0.383}	—	0
20190330A	204.09	38.36	509.5	25.4	434.1	1.14 ± 0.21	0.458 ^{+0.150} _{-0.273}	39.498 ^{+0.348} _{-0.949}	0
20190330B	269.41	52.81	668.0	48.8	569.2	5.30 ± 1.60	0.639 ^{+0.158} _{-0.339}	40.487 ^{+0.329} _{-0.884}	1
20190401A	196.80	79.91	779.6	38.8	690.8	8.60 ± 3.00	0.791 ^{+0.171} _{-0.326}	40.904 ^{+0.318} _{-0.700}	1
20190402A	178.61	47.10	1287.5	22.2	1215.3	1.34 ± 0.52	1.453 ^{+0.246} _{-0.379}	40.678 ^{+0.289} _{-0.500}	0

— Continued from previous page

FRBs	RA [°]	Dec [°]	DM _{obs} [pc/cm ³]	DM _{MW} [pc/cm ³]	DM _E [pc/cm ³]	Fluence [Jy ms]	z_{inf}	$\log(E/\text{erg})$	flag
20190403A	116.33	86.36	519.2	54.6	414.6	3.19±0.86	0.435 ^{+0.145} _{-0.275}	39.894 ^{+0.382} _{-1.083}	0
20190403B	135.47	1.46	291.1	52.7	188.4	23.80±6.80	0.126 ^{+0.119} _{-0.096}	39.603 ^{+0.728} _{-1.437}	1
20190403C	249.83	58.70	933.3	37.2	846.1	1.53±0.33	0.983 ^{+0.198} _{-0.326}	40.364 ^{+0.261} _{-0.494}	0
20190403D	326.53	84.29	613.0	62.5	500.5	1.75±0.56	0.547 ^{+0.150} _{-0.303}	39.855 ^{+0.355} _{-0.938}	0
20190403E	220.22	86.54	220.0	43.7	126.3	76.00±25.00	0.051 ^{+0.097} _{-0.046}	39.300 ^{+1.084} _{-2.182}	0
20190403F	43.34	33.14	666.4	69.6	546.8	7.10±2.40	0.613 ^{+0.151} _{-0.331}	40.574 ^{+0.340} _{-0.926}	0
20190403G	81.74	25.78	865.4	165.4	650.0	1.59±0.44	0.737 ^{+0.167} _{-0.307}	40.102 ^{+0.304} _{-0.661}	0
20190404A	143.10	36.90	1353.8	40.2	1263.6	4.50±1.80	1.513 ^{+0.256} _{-0.384}	41.242 ^{+0.291} _{-0.499}	1
20190404B	259.79	40.00	490.1	45.7	394.4	16.30±3.20	0.410 ^{+0.140} _{-0.277}	40.547 ^{+0.361} _{-1.150}	1
20190405A	337.02	20.96	423.8	46.2	327.6	2.50±1.30	0.310 ^{+0.145} _{-0.225}	39.465 ^{+0.549} _{-1.520}	0
20190405B	236.48	89.16	1111.2	51.9	1009.3	17.50±6.30	1.195 ^{+0.208} _{-0.363}	41.609 ^{+0.285} _{-0.542}	1
20190408A	262.20	71.60	862.1	44.7	767.4	1.51±0.68	0.879 ^{+0.192} _{-0.311}	40.250 ^{+0.351} _{-0.683}	0
20190409A	79.52	6.72	1789.0	81.5	1657.5	8.70±2.80	2.026 ^{+0.305} _{-0.495}	41.798 ^{+0.249} _{-0.428}	1
20190409B	126.65	63.47	297.6	59.8	187.8	6.80±2.50	0.125 ^{+0.119} _{-0.095}	39.052 ^{+0.757} _{-1.491}	0
20190409C	252.60	71.62	674.5	42.9	581.6	2.17±0.94	0.653 ^{+0.161} _{-0.328}	40.120 ^{+0.369} _{-0.919}	0
20190409D	336.64	26.95	1298.9	53.5	1195.4	2.74±0.69	1.427 ^{+0.239} _{-0.377}	40.971 ^{+0.242} _{-0.418}	1
20190410A	263.47	-2.37	278.2	122.7	105.5	5.80±1.60	0.028 ^{+0.087} _{-0.027}	37.649 ^{+1.364} _{-3.049}	0
20190410B	265.76	15.17	642.1	78.3	513.8	0.45±0.15	0.567 ^{+0.149} _{-0.312}	39.300 ^{+0.351} _{-0.941}	1
20190411A	80.00	83.89	461.0	61.2	349.8	1.41±0.51	0.344 ^{+0.141} _{-0.251}	39.316 ^{+0.464} _{-1.407}	0
20190411B	154.03	29.23	1227.7	33.4	1144.3	3.70±0.57	1.361 ^{+0.224} _{-0.384}	41.058 ^{+0.205} _{-0.389}	1
20190411C	9.33	20.50	234.5	39.7	144.8	9.30±2.40	0.072 ^{+0.107} _{-0.059}	38.690 ^{+0.928} _{-1.676}	1
20190412A	243.45	61.87	363.9	36.7	277.2	6.90±2.20	0.245 ^{+0.138} _{-0.180}	39.684 ^{+0.545} _{-1.386}	1
20190412B	285.65	19.25	375.3	264.4	60.9	12.80±5.20	—	—	0
20190414A	181.44	38.90	812.0	20.2	741.8	1.74±0.48	0.850 ^{+0.184} _{-0.331}	40.280 ^{+0.294} _{-0.617}	1
20190414B	246.90	57.53	511.1	42.4	418.7	3.80±1.00	0.440 ^{+0.147} _{-0.275}	39.981 ^{+0.379} _{-1.059}	1
20190415A	182.38	71.28	632.4	35.7	546.7	3.70±1.40	0.613 ^{+0.151} _{-0.331}	40.291 ^{+0.353} _{-0.953}	1
20190415B	8.86	54.85	711.7	144.1	517.6	22.30±3.40	0.573 ^{+0.149} _{-0.315}	41.005 ^{+0.286} _{-0.835}	0
20190415C	74.81	34.80	648.6	166.9	431.7	0.77±0.19	0.455 ^{+0.150} _{-0.274}	39.321 ^{+0.371} _{-0.994}	0
20190416A	144.99	33.30	2287.1	39.0	2198.1	2.80±0.86	2.790 ^{+0.390} _{-0.612}	41.593 ^{+0.231} _{-0.381}	1
20190416B	172.19	35.95	574.2	19.4	504.8	1.47±0.53	0.553 ^{+0.150} _{-0.306}	39.791 ^{+0.365} _{-0.963}	1
20190417B	174.87	64.72	1151.7	25.5	1076.2	9.90±1.80	1.276 ^{+0.222} _{-0.398}	41.424 ^{+0.224} _{-0.445}	0
20190417C	45.68	71.26	318.6	120.4	148.2	10.80±4.90	0.076 ^{+0.108} _{-0.062}	38.801 ^{+0.973} _{-1.766}	1
20190418A	65.79	16.04	182.8	68.4	64.4	2.20±1.00	—	—	1
20190419A	104.98	64.88	438.3	60.6	327.7	0.77±0.30	0.310 ^{+0.145} _{-0.226}	38.954 ^{+0.510} _{-1.415}	0
20190419B	255.27	86.74	166.6	53.8	62.8	7.90±3.50	—	—	1
20190420A	106.55	55.96	609.8	66.4	493.4	3.11±0.61	0.536 ^{+0.151} _{-0.298}	40.086 ^{+0.318} _{-0.869}	1
20190420B	94.73	70.12	844.3	64.9	729.4	15.10±6.70	0.836 ^{+0.180} _{-0.337}	41.202 ^{+0.348} _{-0.755}	1
20190420C	248.10	37.25	627.6	33.4	544.2	4.13±0.96	0.610 ^{+0.151} _{-0.331}	40.334 ^{+0.305} _{-0.864}	0
20190421B	82.49	62.31	393.1	97.3	245.8	16.40±4.90	0.206 ^{+0.127} _{-0.153}	39.895 ^{+0.567} _{-1.398}	1
20190422A	48.56	35.15	452.9	80.1	322.8	9.10±2.80	0.303 ^{+0.146} _{-0.220}	40.003 ^{+0.493} _{-1.358}	1
20190422B	158.27	45.67	975.4	32.1	893.3	1.57±0.55	1.047 ^{+0.198} _{-0.346}	40.435 ^{+0.296} _{-0.574}	0
20190423A	179.68	55.25	244.2	33.2	161.0	55.40±8.80	0.090 ^{+0.115} _{-0.071}	39.667 ^{+0.817} _{-1.461}	1

— Continued from previous page

FRBs	RA [°]	Dec [°]	DM _{obs} [pc/cm ³]	DM _{MW} [pc/cm ³]	DM _E [pc/cm ³]	Fluence [Jy ms]	z_{inf}	$\log(E/\text{erg})$	flag
20190423B	298.58	26.19	585.5	483.2	52.3	7.00 ± 1.30	—	—	0
20190423C	349.08	86.97	855.7	60.6	745.1	4.37 ± 0.97	0.854 ^{+0.185} _{-0.328}	40.684 ^{+0.276} _{-0.578}	1
20190423D	29.69	84.80	498.2	67.9	380.3	18.00 ± 6.80	0.391 ^{+0.138} _{-0.276}	40.545 ^{+0.430} _{-1.349}	1
20190424A	168.30	63.78	758.6	35.4	673.2	1.99 ± 0.58	0.768 ^{+0.169} _{-0.317}	40.239 ^{+0.303} _{-0.666}	1
20190425A	255.72	21.52	127.8	48.4	29.4	31.60 ± 4.20	—	—	1
20190425B	210.12	88.60	1030.3	51.3	929.0	3.10 ± 1.30	1.094 ^{+0.198} _{-0.344}	40.773 ^{+0.310} _{-0.600}	1
20190426A	115.04	59.12	341.3	56.5	234.8	2.01 ± 0.29	0.191 ^{+0.124} _{-0.143}	38.914 ^{+0.529} _{-1.319}	1
20190427A	78.93	7.77	454.5	83.7	320.8	9.50 ± 2.90	0.300 ^{+0.146} _{-0.218}	40.013 ^{+0.495} _{-1.356}	1
20190428A	170.73	23.33	968.9	26.5	892.4	7.40 ± 2.20	1.046 ^{+0.198} _{-0.346}	41.108 ^{+0.279} _{-0.540}	1
20190429A	281.09	59.42	470.7	57.4	363.3	1.83 ± 0.31	0.365 ^{+0.139} _{-0.266}	39.485 ^{+0.378} _{-1.298}	0
20190429B	329.93	3.96	297.6	44.1	203.5	5.00 ± 1.60	0.147 ^{+0.120} _{-0.111}	39.068 ^{+0.679} _{-1.440}	0
20190430A	77.70	87.01	349.4	68.0	231.4	7.70 ± 2.30	0.186 ^{+0.123} _{-0.139}	39.473 ^{+0.591} _{-1.407}	0
20190430B	237.72	62.27	2617.1	34.1	2533.0	1.52 ± 0.52	3.278 ^{+0.449} _{-0.650}	41.470 ^{+0.239} _{-0.377}	0
20190430C	277.22	24.92	399.5	98.0	251.5	5.10 ± 1.20	0.213 ^{+0.129} _{-0.158}	39.420 ^{+0.539} _{-1.355}	1
20190501B	261.45	54.36	784.5	44.0	690.5	3.20 ± 0.55	0.791 ^{+0.171} _{-0.326}	40.474 ^{+0.257} _{-0.595}	1
20190502A	165.01	59.95	626.0	35.2	540.8	11.50 ± 2.30	0.606 ^{+0.150} _{-0.329}	40.772 ^{+0.293} _{-0.849}	1
20190502B	212.04	64.44	917.1	32.3	834.8	10.10 ± 1.60	0.967 ^{+0.198} _{-0.321}	41.168 ^{+0.242} _{-0.464}	1
20190502C	155.60	82.97	396.3	46.9	299.4	8.30 ± 3.50	0.273 ^{+0.143} _{-0.199}	39.865 ^{+0.555} _{-1.445}	1
20190515A	310.15	55.46	452.9	159.8	243.1	16.80 ± 1.80	0.202 ^{+0.126} _{-0.151}	39.890 ^{+0.500} _{-1.296}	0
20190515B	0.83	3.41	820.1	30.4	739.7	11.30 ± 4.80	0.848 ^{+0.183} _{-0.332}	41.089 ^{+0.342} _{-0.722}	1
20190515D	67.13	-5.01	425.4	47.1	328.3	8.80 ± 4.40	0.311 ^{+0.145} _{-0.226}	40.015 ^{+0.542} _{-1.502}	1
20190516B	167.34	7.37	1235.8	33.7	1152.1	9.90 ± 5.30	1.371 ^{+0.224} _{-0.377}	41.492 ^{+0.328} _{-0.639}	1
20190517C	87.50	26.62	334.8	187.2	97.6	8.70 ± 2.80	—	—	0
20190517D	339.95	41.84	1184.0	97.2	1036.8	5.80 ± 3.00	1.228 ^{+0.214} _{-0.378}	41.155 ^{+0.333} _{-0.668}	0
20190518B	175.11	20.28	913.9	26.2	837.7	2.10 ± 1.00	0.972 ^{+0.198} _{-0.322}	40.490 ^{+0.347} _{-0.670}	1
20190518C	242.01	4.64	444.8	42.4	352.4	14.80 ± 3.30	0.348 ^{+0.141} _{-0.254}	40.348 ^{+0.413} _{-1.323}	1
20190518D	174.72	89.31	202.2	53.7	98.5	3.00 ± 1.60	—	—	1
20190518G	94.79	75.52	525.7	63.8	411.9	1.76 ± 0.62	0.431 ^{+0.145} _{-0.275}	39.629 ^{+0.410} _{-1.148}	1
20190519D	164.57	42.99	538.6	29.3	459.3	0.81 ± 0.36	0.488 ^{+0.154} _{-0.277}	39.411 ^{+0.424} _{-1.053}	1
20190519E	168.28	41.65	693.9	27.6	616.3	1.46 ± 0.67	0.693 ^{+0.166} _{-0.292}	40.006 ^{+0.372} _{-0.795}	1
20190519F	165.63	77.23	799.0	43.3	705.7	4.00 ± 1.30	0.809 ^{+0.173} _{-0.331}	40.594 ^{+0.309} _{-0.680}	1
20190519G	306.68	72.34	433.5	76.9	306.6	22.00 ± 12.00	0.282 ^{+0.144} _{-0.206}	40.320 ^{+0.583} _{-1.546}	0
20190519H	342.99	87.37	1169.5	58.0	1061.5	6.60 ± 3.30	1.258 ^{+0.219} _{-0.390}	41.234 ^{+0.328} _{-0.657}	1
20190519J	296.21	86.93	642.1	55.4	536.7	1.70 ± 1.10	0.601 ^{+0.148} _{-0.328}	39.934 ^{+0.430} _{-1.208}	0
20190520A	273.52	26.32	431.9	79.1	302.8	2.40 ± 1.00	0.277 ^{+0.144} _{-0.202}	39.341 ^{+0.550} _{-1.439}	1
20190527A	12.45	7.99	582.3	31.4	500.9	10.10 ± 4.10	0.548 ^{+0.150} _{-0.303}	40.618 ^{+0.383} _{-0.997}	1
20190527C	100.22	57.00	535.4	73.8	411.6	20.00 ± 12.00	0.431 ^{+0.145} _{-0.275}	40.683 ^{+0.483} _{-1.359}	1
20190529A	68.06	40.32	703.6	164.6	489.0	1.45 ± 0.49	0.530 ^{+0.152} _{-0.295}	39.743 ^{+0.371} _{-0.955}	0
20190530A	68.74	60.59	554.8	138.6	366.2	1.69 ± 0.90	0.370 ^{+0.139} _{-0.270}	39.463 ^{+0.492} _{-1.549}	0
20190531A	203.96	81.72	325.1	44.4	230.7	—	0.185 ^{+0.123} _{-0.139}	—	0
20190531B	259.91	49.32	166.6	41.7	74.9	—	—	—	0
20190531C	331.14	43.00	477.2	131.4	295.8	1.20 ± 1.00	0.268 ^{+0.143} _{-0.196}	39.010 ^{+0.670} _{-1.987}	0

— Continued from previous page

FRBs	RA [°]	Dec [°]	DM _{obs} [pc/cm ³]	DM _{MW} [pc/cm ³]	DM _E [pc/cm ³]	Fluence [Jy ms]	z_{inf}	$\log(E/\text{erg})$	flag
20190531E	15.20	0.54	328.4	32.2	246.2	5.30 ± 2.90	0.206 ^{+0.127} _{-0.154}	39.407 ^{+0.642} _{-1.588}	0
20190601A	190.11	62.72	2228.9	34.0	2144.9	2.70 ± 2.40	2.703 ^{+0.380} _{-0.582}	41.550 ^{+0.392} _{-1.172}	1
20190601B	17.88	23.82	789.3	43.4	695.9	13.00 ± 3.90	0.798 ^{+0.171} _{-0.328}	41.092 ^{+0.301} _{-0.667}	1
20190601C	88.52	28.47	423.8	186.1	187.7	5.80 ± 2.50	0.125 ^{+0.119} _{-0.095}	38.982 ^{+0.778} _{-1.537}	0
20190601D	85.86	79.35	669.6	65.0	554.6	5.70 ± 1.70	0.622 ^{+0.154} _{-0.334}	40.493 ^{+0.327} _{-0.894}	0
20190603B	48.87	74.28	503.0	99.0	354.0	6.20 ± 2.70	0.351 ^{+0.140} _{-0.256}	39.977 ^{+0.480} _{-1.462}	0
20190604C	77.39	49.30	504.7	153.0	301.7	26.20 ± 4.20	0.276 ^{+0.144} _{-0.201}	40.375 ^{+0.464} _{-1.282}	0
20190604D	199.93	15.73	1020.6	24.2	946.4	2.48 ± 0.79	1.117 ^{+0.199} _{-0.342}	40.695 ^{+0.276} _{-0.519}	1
20190604E	235.59	32.06	1218.0	25.4	1142.6	2.26 ± 0.82	1.359 ^{+0.224} _{-0.386}	40.842 ^{+0.278} _{-0.514}	1
20190604G	120.81	59.50	231.3	49.7	131.6	4.49 ± 0.75	0.057 ^{+0.100} _{-0.050}	38.169 ^{+0.982} _{-1.891}	1
20190605C	168.32	-5.19	186.0	36.2	99.8	4.40 ± 1.50	—	—	1
20190605D	26.72	28.62	1653.1	45.4	1557.7	2.16 ± 0.84	1.903 ^{+0.289} _{-0.456}	41.136 ^{+0.271} _{-0.469}	0
20190606B	108.79	86.85	275.0	52.6	172.4	17.40 ± 5.40	0.103 ^{+0.118} _{-0.080}	39.287 ^{+0.820} _{-1.484}	1
20190607A	26.23	23.66	559.7	41.2	468.5	21.30 ± 3.70	0.499 ^{+0.155} _{-0.281}	40.853 ^{+0.331} _{-0.870}	1
20190607B	42.02	49.62	289.5	138.4	101.1	3.20 ± 0.61	0.023 ^{+0.085} _{-0.022}	37.222 ^{+1.445} _{-2.831}	1
20190608A	359.23	19.17	719.8	36.0	633.8	1.51 ± 0.59	0.715 ^{+0.167} _{-0.299}	40.051 ^{+0.346} _{-0.738}	0
20190609A	345.30	87.94	315.4	57.2	208.2	10.40 ± 4.10	0.153 ^{+0.121} _{-0.116}	39.426 ^{+0.686} _{-1.486}	0
20190609B	210.49	88.35	292.8	52.9	189.9	22.20 ± 8.40	0.128 ^{+0.119} _{-0.098}	39.587 ^{+0.751} _{-1.496}	1
20190609C	73.17	24.06	480.4	112.8	317.6	1.91 ± 0.43	0.296 ^{+0.145} _{-0.215}	39.303 ^{+0.471} _{-1.310}	0
20190609D	115.94	51.69	509.5	55.3	404.2	2.36 ± 0.94	0.422 ^{+0.143} _{-0.276}	39.735 ^{+0.426} _{-1.220}	1
20190612A	148.16	70.42	427.0	36.4	340.6	20.00 ± 10.00	0.330 ^{+0.143} _{-0.240}	40.428 ^{+0.521} _{-1.509}	0
20190612B	222.21	4.31	186.0	26.1	109.9	3.78 ± 0.68	0.033 ^{+0.089} _{-0.032}	37.606 ^{+1.243} _{-3.137}	0
20190612C	79.12	61.01	1638.5	104.7	1483.8	12.10 ± 3.20	1.804 ^{+0.275} _{-0.441}	41.835 ^{+0.232} _{-0.395}	0
20190613A	257.40	18.85	714.9	53.4	611.5	8.00 ± 3.20	0.688 ^{+0.165} _{-0.296}	40.737 ^{+0.355} _{-0.766}	0
20190613B	65.75	42.67	286.3	170.0	66.3	1.26 ± 0.27	—	—	0
20190614A	179.79	88.33	1062.7	51.0	961.7	2.21 ± 0.93	1.136 ^{+0.201} _{-0.340}	40.662 ^{+0.307} _{-0.580}	0
20190614B	332.86	24.69	580.7	53.7	477.0	8.40 ± 2.80	0.512 ^{+0.154} _{-0.286}	40.472 ^{+0.380} _{-0.958}	1
20190614C	356.50	35.91	585.5	53.8	481.7	2.91 ± 0.95	0.519 ^{+0.153} _{-0.290}	40.025 ^{+0.373} _{-0.951}	1
20190616A	234.03	34.48	211.9	24.8	137.1	1.67 ± 0.55	0.063 ^{+0.103} _{-0.054}	37.830 ^{+0.999} _{-1.849}	0
20190617A	178.60	83.87	195.7	46.6	99.1	21.00 ± 9.30	—	—	0
20190617B	56.43	1.16	275.0	45.3	179.7	9.20 ± 4.70	0.113 ^{+0.119} _{-0.087}	39.097 ^{+0.840} _{-1.617}	0
20190617C	134.37	35.70	637.3	42.5	544.8	4.10 ± 1.40	0.611 ^{+0.151} _{-0.331}	40.332 ^{+0.341} _{-0.930}	0
20190618A	321.25	25.44	228.1	76.4	101.7	4.30 ± 1.70	0.024 ^{+0.085} _{-0.023}	37.375 ^{+1.497} _{-2.983}	0
20190619A	165.18	68.37	897.7	35.4	812.3	3.33 ± 0.89	0.936 ^{+0.198} _{-0.310}	40.654 ^{+0.287} _{-0.524}	0
20190619B	231.74	82.15	270.1	45.4	174.7	4.50 ± 1.60	0.106 ^{+0.118} _{-0.082}	38.728 ^{+0.821} _{-1.508}	0
20190619C	38.29	36.33	486.9	67.9	369.0	1.22 ± 0.37	0.374 ^{+0.139} _{-0.273}	39.332 ^{+0.418} _{-1.377}	0
20190619D	114.79	41.59	375.3	60.8	264.5	6.50 ± 1.60	0.229 ^{+0.134} _{-0.169}	39.594 ^{+0.531} _{-1.351}	0
20190621B	193.14	55.64	1059.5	29.0	980.5	1.19 ± 0.38	1.159 ^{+0.204} _{-0.348}	40.412 ^{+0.274} _{-0.510}	0
20190621C	206.57	5.23	571.0	26.4	494.6	2.38 ± 0.54	0.538 ^{+0.151} _{-0.299}	39.973 ^{+0.328} _{-0.885}	1
20190621D	270.63	78.89	645.4	48.6	546.8	4.30 ± 1.90	0.613 ^{+0.151} _{-0.331}	40.356 ^{+0.373} _{-1.000}	1
20190622A	298.98	85.81	1120.9	54.9	1016.0	1.28 ± 0.58	1.203 ^{+0.209} _{-0.367}	40.479 ^{+0.314} _{-0.611}	0
20190623A	270.48	24.52	1082.1	74.1	958.0	0.86 ± 0.19	1.131 ^{+0.201} _{-0.341}	40.248 ^{+0.242} _{-0.453}	0

— Continued from previous page

FRBs	RA [°]	Dec [°]	DM _{obs} [pc/cm ³]	DM _{MW} [pc/cm ³]	DM _E [pc/cm ³]	Fluence [Jy ms]	z_{inf}	$\log(E/\text{erg})$	flag
20190623B	335.22	46.12	1554.4	141.4	1363.0	2.78 ± 0.87	$1.627^{+0.282}_{-0.400}$	$41.100^{+0.266}_{-0.429}$	1
20190623C	192.31	86.03	1049.8	48.8	951.0	5.90 ± 1.70	$1.122^{+0.200}_{-0.342}$	$41.077^{+0.266}_{-0.497}$	1
20190624A	168.32	69.78	973.7	37.7	886.0	3.01 ± 0.98	$1.037^{+0.198}_{-0.343}$	$40.709^{+0.289}_{-0.558}$	1
20190624B	304.65	73.61	215.1	70.9	94.2	20.00 ± 5.20	—	—	1
20190625A	227.91	32.88	297.6	18.6	229.0	11.90 ± 2.70	$0.183^{+0.123}_{-0.137}$	$39.645^{+0.571}_{-1.366}$	0
20190625C	73.20	11.10	441.6	75.5	316.1	4.02 ± 0.83	$0.294^{+0.145}_{-0.214}$	$39.621^{+0.465}_{-1.300}$	1
20190625D	115.02	4.87	716.6	100.1	566.5	12.10 ± 2.10	$0.636^{+0.157}_{-0.338}$	$40.841^{+0.284}_{-0.813}$	1
20190627A	195.89	0.75	402.8	28.9	323.9	2.62 ± 0.68	$0.304^{+0.145}_{-0.221}$	$39.468^{+0.474}_{-1.329}$	0
20190627B	256.40	40.79	428.6	40.3	338.3	10.20 ± 1.40	$0.327^{+0.143}_{-0.238}$	$40.125^{+0.404}_{-1.271}$	1
20190627C	267.88	71.58	968.9	48.3	870.6	11.30 ± 4.00	$1.017^{+0.198}_{-0.337}$	$41.264^{+0.302}_{-0.578}$	1
20190627D	295.33	43.84	1999.2	129.0	1820.2	1.54 ± 0.28	$2.244^{+0.343}_{-0.507}$	$41.139^{+0.200}_{-0.321}$	1
20190628A	199.06	51.75	745.7	29.7	666.0	1.28 ± 0.32	$0.758^{+0.168}_{-0.314}$	$40.036^{+0.291}_{-0.642}$	0
20190628B	248.48	80.14	406.0	44.5	311.5	1.39 ± 0.34	$0.288^{+0.145}_{-0.210}$	$39.141^{+0.484}_{-1.323}$	1
20190628C	11.52	48.59	1740.4	90.8	1599.6	2.45 ± 0.62	$1.954^{+0.295}_{-0.472}$	$41.215^{+0.226}_{-0.383}$	0
20190629A	6.34	12.67	503.0	34.3	418.7	3.05 ± 0.76	$0.440^{+0.147}_{-0.275}$	$39.885^{+0.375}_{-1.051}$	0
20190630B	328.21	43.01	653.5	151.9	451.6	14.70 ± 1.80	$0.479^{+0.153}_{-0.274}$	$40.651^{+0.318}_{-0.864}$	0
20190630C	68.38	80.95	1659.6	67.3	1542.3	2.27 ± 0.83	$1.883^{+0.285}_{-0.449}$	$41.147^{+0.264}_{-0.451}$	0
20190630D	143.36	8.90	321.9	42.1	229.8	2.60 ± 0.75	$0.184^{+0.123}_{-0.138}$	$38.991^{+0.591}_{-1.401}$	1
20190701A	277.47	59.04	635.7	52.9	532.8	1.70 ± 0.29	$0.596^{+0.148}_{-0.325}$	$39.925^{+0.284}_{-0.839}$	1
20190701B	302.93	80.18	748.9	61.3	637.6	1.90 ± 0.72	$0.720^{+0.167}_{-0.301}$	$40.158^{+0.341}_{-0.729}$	1
20190701C	96.36	81.63	972.1	56.3	865.8	2.50 ± 1.60	$1.010^{+0.198}_{-0.335}$	$40.603^{+0.386}_{-0.832}$	0
20190701D	112.10	66.70	934.9	57.5	827.4	8.60 ± 3.60	$0.957^{+0.198}_{-0.317}$	$41.088^{+0.332}_{-0.624}$	1
20190701E	138.57	61.71	888.0	39.9	798.1	2.00 ± 0.49	$0.916^{+0.198}_{-0.303}$	$40.412^{+0.283}_{-0.511}$	1